Journal of Statistical Physics, Vol. 116, No. 5/6, September 2004 (© 2004)

Discrete Charges on a Two Dimensional Conductor

Marko Kleine Berkenbusch,[1] Isabelle Claus,[1] Catherine Dunn,[1] Leo P. Kadanoff,[1] Maciej Nicewicz,[1] and Shankar C. Venkataramani[1]

Received October 10, 2003; accepted March 25, 2004

We investigate the electrostatic equilibria of N discrete charges of size $1/N$ on a two dimensional conductor (domain). We study the distribution of the charges on symmetric domains including the ellipse, the hypotrochoid and various regular polygons, with an emphasis on understanding the distributions of the charges, as the shape of the underlying conductor becomes singular. We find that there are two regimes of behavior, a symmetric regime for smooth conductors, and a symmetry broken regime for "singular" domains. For smooth conductors, the locations of the charges can be determined, to within $O(\sqrt{\log N}/N^2)$ by an integral equation due to Pommerenke [*Math. Ann.*, **179**: 212–218, (1969)]. We present a derivation of a related (but different) integral equation, which has the same solutions. We also solve the equation to obtain (asymptotic) solutions which show universal behavior in the distribution of the charges in conductors with somewhat smooth cusps. Conductors with sharp cusps and singularities show qualitatively different behavior, where the symmetry of the problem is broken, and the distribution of the discrete charges does not respect the symmetry of the underlying domain. We investigate the symmetry breaking both theoretically, and numerically, and find good agreement between our theory and the numerics. We also find that the universality in the distribution of the charges near the cusps *persists* in the symmetry broken regime, although this distribution is very different from the one given by the integral equation.

KEY WORDS: Fekete points; singular domains; symmetry breaking; electrostatic equilibrium.

[1]The Materials Research Science and Engineering Center, The University of Chicago, 5640 S. Ellis Avenue, Chicago, Illinois 60637, USA, e-mail: mkb@uchicago.edu

0022-4715/04/0900-1301/0

1. INTRODUCTION

The placement of charges on a conductor is a classical problem in both physics and mathematics. In physics the history of the problem goes back to the work of J.J. Thomson.[35,7,6] The placement of charges on a line was investigated by Stieltjes[33] in the late 19th century. Fekete[13] recognized the connection between the placement of charges on a 2 dimensional domain, and questions involving polynomial functions of a complex variable. This problem was also investigated by Frostman,[14] for its connections to Potential theory. In general, the problem is to place N charges of strength $1/N$ on a surface so that the energy is minimized. In this placement the force component parallel to the surface for each charge vanishes.

This problem has quite a different nature depending upon the dimension of the system. In three dimensional space, one uses an inverse square force law. The placement upon any surface, even one as simple as the surface of a sphere is quite complex. The discrete charges form an approximation of a lattice with many defects.[11,7,6,8] The solution might properly be described as being chaotic.

In contrast, in two dimensions, one finds smoother behavior. The problem is one of placement of lines of charge on the curve which bounds a two- dimensional conductor. Forces between the charges are given by an inverse first power of the distance.

The analogous continuum problem has a very good general formulation via the Riemann mapping theorem. To calculate the distribution of continuum charges on the exterior of a simply connected region in the plane, construct the unique function $F(w)$ that takes the exterior of the unit circle into the exterior of the region, and has the property that $F(w) \to w$ as $w \to \infty$. Then the density of charges at the point $z = F(w) = F(e^{i\theta})$ on the surface of the conductor is given by

$$\rho(\theta) = |wF'(w)|^{-1} \tag{1}$$

This result provides the basis for all subsequent work on discrete charges.

More recent work[22–24] has looked at the placement of discrete charges in terms of the placement of points on the circle at

$$w_j = e^{2\pi i\theta_j} \tag{2}$$

The θ_j's are real. According to a set of important recent theorems,[23] for sufficiently smooth curves C, we can determine the charge placement for all large enough values of N in terms of a smooth periodic function,

$\psi(\theta)$[2], by writing

$$\theta_j \approx \theta_0 + \frac{2\pi j}{N} + \frac{1}{N}\left[\psi\left(\theta_0 + \frac{2\pi j}{N}\right) - \psi(\theta_0)\right] \tag{3}$$

With appropriate choice of θ_0, expression 3 gives the placement of charges with error of order $\sqrt{\log(N)}/N^{2(29)}$ for all extrema of the energy

$$E^N(\{\theta\}) = -\frac{1}{2N^2}\sum_{j\neq k} \Re \ \ln[F(w_j) - F(w_k)] \tag{4}$$

Here we represent the usual logarithmic potential for line-charges by taking the real part of the complex logarithm function.

1.1. New Empirical Results

We calculate the actual position of charges on two different kinds of shapes: ellipses and hypotrochoids. These two kinds of shapes are defined as the image of the unit circle under maps of the form

$$F(w) = w - \frac{c}{w^r} \tag{5}$$

Here $r = 1$ for ellipses and $r = 2$ for hypotrochoids. The parameter c controls how different these figures are from the circle.

Results of these mappings are shown in figures 1,2. These figures also include the positions of the charges placed upon these conductors. As one might expect from equation 1, the charge densities are highest in the high curvature areas of the bounding curves. However, the figures also contain some surprises. In both cases, there is a symmetry breaking in the more pointed figures. In this breaking, the left-right symmetry is broken at each pointy region, and the overall parity symmetry of the figure is lost. We shall explore this symmetry-breaking in more detail below.

To understand these charge placements, look at the energies they generate. When the sizes of the figures are properly adjusted the continuum correlation energy is zero. The next term in the energy is the self-energy:

$$E_s^N = -\frac{\ln N}{2N} \tag{6}$$

[2]This functional is conventionally denoted by Φ. We however reserve Φ for the electrostatic potential.

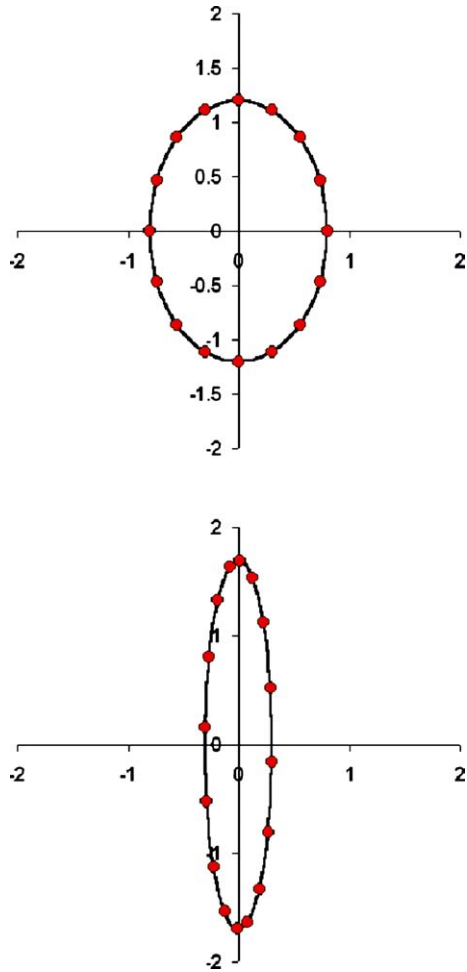

Fig. 1. Placement of 16 charges on two different ellipses, $c = 0.2$ and $c = 0.7$ respectively. Notice the breaking of the parity symmetry in part b. The ellipse degenerates to a line when $c = 1$.

This term is independent of charge placement. The remaining energy is a correlation energy, and has a power-law behavior in N for large N:

$$E_c^N \sim N^{-s} \tag{7}$$

Here the exponent s is known to be two for smooth curves. In figure 3 we plot the correlation energy versus N for three different hypotrochoids.

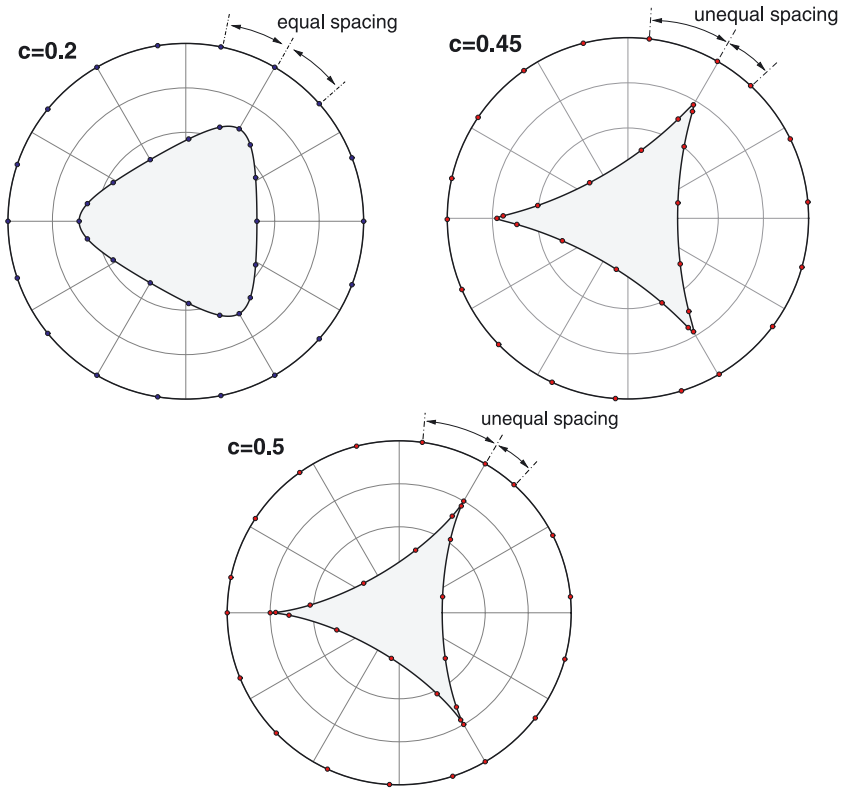

Fig. 2. Placement of 18 charges on three different hypotrochoids, corresponding to $c=0.2$, $c=0.45$ and $c=0.5$ respectively. Notice the breaking of the parity symmetry in part b and c. The hypotrochoid is smooth for $0 \leqslant c < 1/2$ but gains three pointed cusps at $c=1/2$.

In the first case, we can clearly see that $s=2$. For the singular figure, corresponding to figure 2c, the log-log plot exhibits a slope of 1.5. In the intermediate case, corresponding to the blunted points of figure 2b, there is a crossover from $s=1.5$ for smaller N to $s=2$ for larger N.

1.2. Connection to Modern Work in Dynamical Systems Theory

Note the close connection between equation 3 and the expression giving the positions of points in long cycles and quasi-periodic orbits of KAM[5] theory. KAM theory provides an expansion about continuum motion, in which the positioning of points in a cycle closely follows that of the corresponding continuum orbit. In this Coulomb system too, a near

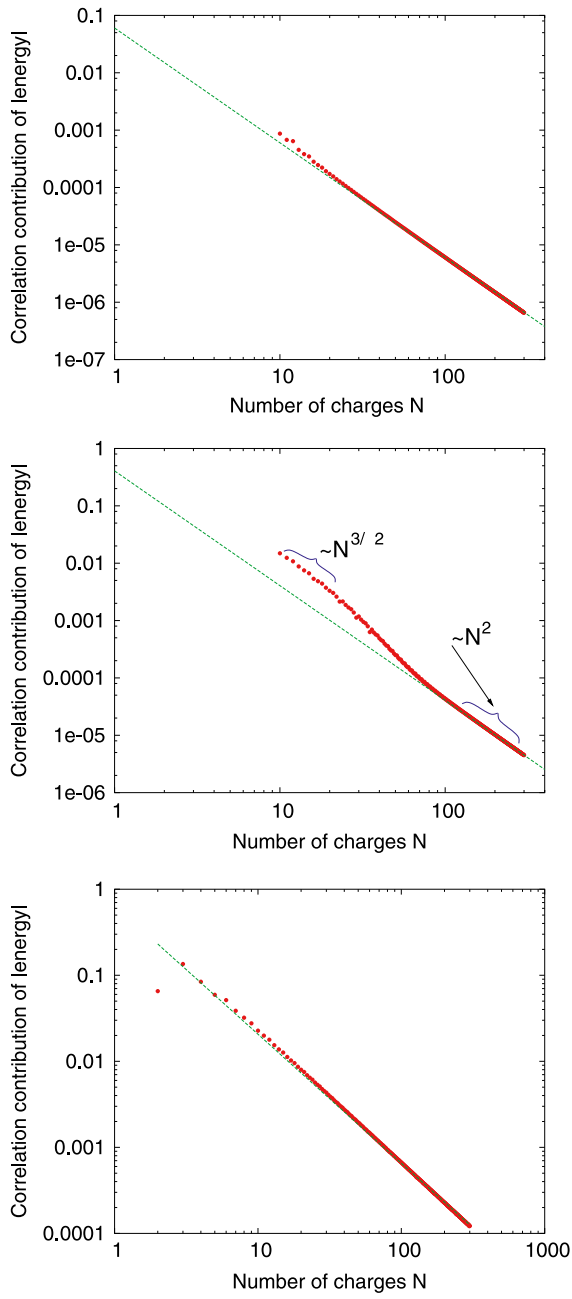

Fig. 3. Plot of correlation energy versus N. The three curves shown correspond to the three hypotrochoids shown in figure 2.

continuum result gives a charge density which is only a little different from the one in the continuum case. As in KAM theory, equation 3 describes a near-continuum result by giving a function, here ψ, which describes the deviation from and permits a smooth passage to the continuum limit in which N goes to infinity.

In KAM theory, the cycles closely follow a continuum orbit. So the continuum theory predicts the curve on which the points will occur; but it does not give the positioning of the points in the orbit. A more subtle calculation is required to find that. Here the analogous fact is that the initial angle θ_0 of equation 3 is not determined by any continuum theory. In fact, one does not know a first principles method of finding θ_0.

Dynamical systems theory is much concerned with bifurcations, *i.e.*, situations in which a qualitative change in behavior occurs. In the Coulomb problem there is a bifurcation from the single *symmetric* to multiple solutions and symmetry breaking behavior. In dynamical systems theory when a parameter is varied, bifurcations can occur for longer and longer orbits producing an interesting kind of critical behavior.[17,20,21] Here the analogous situation arises when the bounding curve develops cusps as the parameter c is varied, and close to this cusp formation, the Coulomb system exhibits a symmetry breaking bifurcation. This behavior produces interesting anomalies including the cross-over in the N-dependence of the energy.

1.3. Paper Outline

Section 2 of this paper deals with the equations for the placement of charges on the circle and on the circle mapping onto "real space". The uniform placement on the circle gives a correlation energy which goes exponentially to zero for large-N.We derive an integral equation which describes the “continuum” behavior of the deviation of the charges from the uniform placement on the circle. This is related to, but different from, the equation formulated by Pommerenke.[29] Our derivation gives a physical interpretation of the equation as being related to the distortions of fields produced by the discrete charges' self-energy effects.

Section 3 follows the analysis of the integral equation in Fourier space. Here the first quantity of interest is the structure function s_k, which is the Fourier transform of the charge distribution. The equation is solved in the large N-limit for both the ellipse (an old result [28]) and the hypotrochoid–a new result. The solution, involving an elliptic function, is formally very similar in the two cases. We also compare the solutions we obtain with numerical observations, and we find that the Integral equation is not applicable for “singular” shapes, and in the symmetry broken regime.

In Sec. 4, we present new results for the singular limit of the Coulomb problem. We investigate the energy and the charge placement in the symmetry broken regime, i.e., for ellipses with $c \approx 1$, hypotrochoids with $c \approx \frac{1}{2}$. We also study "singular" curves with cusps and corners, viz. the line segment, the hypotrochoid with $c = \frac{1}{2}$ and various regular polygons. We present scaling arguments for the dependence of the energy on N in the singular limit, and use this to obtain scaling laws for the symmetry-breaking transition. We also compare these results with numerical simulations.

2. REAL SPACE ANALYSIS

2.1. On the Circle

We describe our electrostatics problem by using complex variables. Thus a charge of size $1/N$ placed at the point (x_j, y_j) will generate the complex potential at the point (x, y) via the formula

$$\Phi(z) = -\frac{1}{N} \ln(z - z_j)$$

where ln is the complex logarithm and z is $x + iy$. If there are N such charges

$$\Phi(z) = -\frac{1}{N} \sum_{j=1}^{N} \ln(z - z_j) \tag{8}$$

When the N charges are uniformly distributed on a circle of radius one, then the potential is

$$\begin{aligned} \Phi(z) &= -\frac{1}{N} \sum_{j=1}^{N} \ln(z - e^{2\pi i j/N}) \\ &= -\frac{1}{N} \ln(z^N - 1) \end{aligned} \tag{9}$$

Note the elegance of the result of equation (9). In the limit of large N, inside the unit circle z^N is very small, and the potential is well approximated by $\Phi = (-\pi i)/N$. Outside, we find $\Phi = -\ln z$ which is the continuum result. To get the potential seen by the charge at $z = 1$, we have to subtract away the charge potential it produces and use

$$\Phi^0(z) = \frac{1}{N} \ln \frac{z - 1}{z^N - 1} \tag{10}$$

Equation (10) describes the potential upon our charge as the potential produced by the charges on the circle less the potential generated by our charge itself. In the neighborhood of $z=1$, we can evaluate this potential as

$$\Phi^0(z) = -\frac{\ln N}{N} - \frac{N-1}{2N}(z-1) - \frac{(N-1)(N-5)}{24N}(z-1)^2 + \ldots.$$

The total energy of this set of charges is obtained as one half this potential (at $z=1$) times the charge summed over all charges. The result is

$$E_N = -\frac{\log N}{2N} \equiv E_s \tag{11}$$

We previously described this term as a self-energy. More precisely the energy of our charges is the energy generated by a continuous circle of charge, namely zero, minus the energy needed to put together the "missing" portions of the circle. Those portions are the lines of charge counted as not present in expressions like equation (10). These are lines of charge of length $2\pi/N$ not generating potential in the gap around our charge itself. The energy of one such gap is $(\log N)/2N^2$. Subtracting away N such energies gives expression (11).

2.2. Uniform Spacing on the Circle

This polynomial method is elegant but it is difficult to generalize to other curves beyond the circle. A method less elegant but more susceptible to
generalization is to evaluate the potential via the contour integral:

$$\Phi^0(z) = -\int_C \frac{dy}{2\pi i y}\frac{1}{y^N-1}\log(z-y) \tag{12}$$

Here the contour, C, encircles all the poles of $1/(y^N-1)$ except the pole at $y=1$ (See Figure 4). By summing the contributions from the various poles we find the result of equation (9) once more.

An alternative mode of evaluation is to deform the contour to include the poles at zero and one and the branch line which runs from z to infinity. The result is then

$$\Phi^0(z) = \log z + \frac{\log(z-1)}{N} - \frac{1}{N}\int_{z^N}^{\infty}\frac{ds}{s}\frac{1}{s-1} \tag{13}$$

which works out to the result (9) once more.

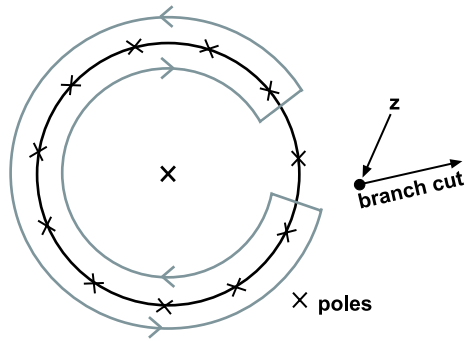

Fig. 4. Contour for calculating the potential generated by $N-1$ charges on the circle.

The next step is to generalize the calculation to include the possibility of a curve other than the unit circle. Let $F(w)$ be the function which conformally maps the exterior of the unit circle into the exterior of a curve C. We shall place our charges on the curve C, but give them the placement which is appropriate for the mapping of charges uniformly spaced on the unit circle. Now consider once more the effect of $N-1$ charges on C. Instead of the integral (12), the potential on a given charge is set by the more general object

$$\Phi_N(z, v) = -\int_C \frac{dw}{2\pi i w} \frac{w^N}{w^N - v^N} \log(z - F(w)) \tag{14}$$

Here v is on the unit circle and the contour, C, encircles the points

$$w_j = v e^{2\pi i j/N} \quad \text{for} \quad j = 1, 2, \ldots, N-1. \tag{15}$$

in the positive sense (See figure 5.) The real part of $\Phi_N(z, v)$ is the potential at the space point z, produced by the specified set of charges. Note that this potential does not take into account the redistribution of charges required to produce an equilibrium distribution.

The calculation follows much the same lines as the previous one, but the details of the calculation are a bit different because the integrand is different. As we move the contour we get four different contributions to the result (14) (See Figure 6). The first contribution comes from the encircling of all the branch lines of the logarithm. The number of the branch lines that connect the preimages of z to 0 depends on the map. The next

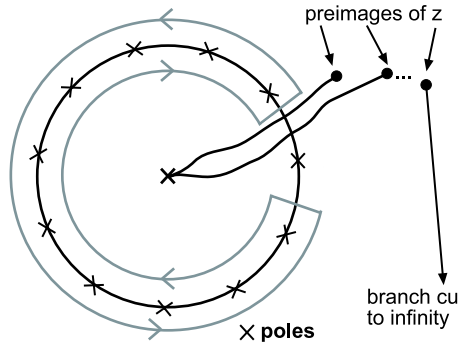

Fig. 5. The contour for equation (14). The main difference from the previous figure is that there are some branch lines within the unit circle. This figure is drawn with $v = 1$.

contribution comes from encircling the pole at $w = v$. This gives a contribution from the "missing" charge, which is

$$\frac{1}{N} \log[z - F(v)]$$

Next comes a contribution from circling the branch line which goes to the point at infinity. Because that encirclement contribution has a logarithmic divergence, we do not carry it out all the way to infinity, but instead cut it off at some large but finite length $L \gg 1$. Then we also need a contribution from a circle at infinity. All this is illustrated in figure 6. The branch

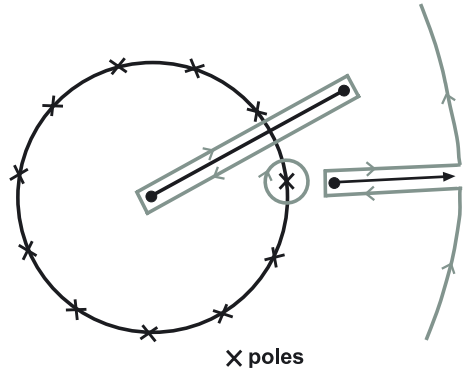

Fig. 6. The contour for equation (14) after deformation.

line contribution is

$$\begin{aligned}\int_{F^{-1}(z)}^{L} \frac{dw}{w}\frac{w^N}{w^N - v^N} &= \frac{1}{N}\int_{[F^{-1}(z)]^N}^{L^N} \frac{du}{u}\frac{u}{u - v^N} \\ &= \frac{1}{N}\ \log\frac{L^N - v^N}{[F^{-1}(z)]^N - v^N} \\ &\approx\ \log L - \frac{1}{N}\log[[F^{-1}(z)]^N - v^N]\end{aligned}$$

Finally, the large circle gives just

$$-\log L$$

since for large w, $F(w)$ is approximately w. When we add up all these terms we see that

$$\Phi_N(z, v) = \frac{1}{N}\log(z - F(v)) - \frac{1}{N}\sum_{u\in F^{-1}\{z\}}\log(u^N - v^N) \tag{16}$$

Equation (16) is a most interesting result. For z inside the curve C, the potential is

$$-\log(-v) + \frac{1}{N}\log[z - F(v)]$$

The first term is an imaginary constant describing how we placed the branch line. The second is a contribution of the "missing" charge. For z outside the the curve C the potential is

$$-\log\ [F^{-1}(z)] + \frac{1}{N}\log[z - F(v)]$$

The first term defines the potential in the limit in which N goes to infinity. This is the familiar but deep statement that the inverse of the mapping is proportional to the exponential of the complex potential. The second term is once more the missing charge.

Finally, we can look at the case in which the potential is evaluated at the unrelaxed position of the Nth charge, i.e. $z = F(v)$. We then have:

$$\Phi_N(F(v), v) = \lim_{z\to F(v)}\Phi_N(z, v) = \lim_{z\to F(v)}\frac{1}{N}\log\left[\frac{z - F(v)}{\prod_{u\in F^{-1}\{z\}}(u^N - v^N)}\right]$$

Clearly, it is $v \in F^{-1}\{F(v)\}$, so all but one part of the limit can be trivially evaluated. The one piece in which $u = v$ can be done by l'Hospital's rule. It then follows that:

$$\Phi_N(F(v), v) = \frac{1}{N} \log\left[\frac{F'(v)}{N v^{N-1}}\right] - \frac{1}{N} \sum_{u \in F^{-1}\{F(v)\}, u \neq v} \log(u^N - v^N) \quad (17)$$

Now we can write down the total energy of the system. Since

$$E_N = \frac{1}{2N} \sum_{j=1}^{N} \Phi_N(F(v_j), v_j)$$

we have

$$\begin{aligned} E_N &= -\frac{\log N}{N} + \frac{1}{2N^2} \sum_j \log\left[\frac{F'(v_j)}{v_j^{N-1}}\right] \\ &\quad - \frac{1}{2N^2} \sum_{j=1}^{N} \sum_{u \in F^{-1}\{F(v)\}, u \neq v} \log(u^N - v^N) \end{aligned}$$

In general, it is difficult to find all such $u's$ and perform the sum. However, in the case of the ellipse given by $F(z) = z + \frac{c}{z}$, this expression nicely simplifies.

2.3. Ellipse Energy – Uniform Spacing

To begin, let us evaluate the first sum in the above expression for the uniform spacing of charges, i.e. put $v_j = \zeta_j$, where ζ_j's are the N^{th} roots of unity.

We have,

$$\frac{1}{2N^2} \sum_{j=1}^{N} \log(\zeta_j F'(\zeta_j)) = \frac{1}{2N^2} \log \prod_{j=1}^{N} \left(\zeta_j - \frac{c}{\zeta_j}\right)$$

It follows that

$$\prod_{j=1}^{N} \left(\zeta_j - \frac{c}{\zeta_j}\right) = (-1)^N \prod_{j=1}^{N} \left(1 - \frac{c}{\zeta_j^2}\right)$$

We notice that since the roots of unity form the cyclic group of order N, and taking N to be odd, 2 always has a multiplicative inverse in $\mathbf{Z}_N$, and the group is invariant under squaring the roots of unity.

Therefore, for odd N,

$$(-1)^N \prod_{j=1}^{N} \left(1 - \frac{c}{\zeta_j^2}\right) = -\prod_{j=1}^{N} \left(1 - \frac{c}{\zeta_j}\right) = -\prod_{j=1}^{N} \left(1 - c\zeta_{N-j}\right)$$

$$= -c^N \prod_{j=1}^{N} \left(\frac{1}{c} - \zeta_{N-j}\right) = -(1 - c^N)$$

It follows

$$\frac{1}{2N^2} \sum_{j=1}^{N} \log(\zeta_j F'(\zeta_j)) = \frac{1}{2N^2} \log(1 - c^N)$$

If N is even, then $2 * \mathbf{Z}_N \cong \mathbf{Z}_{N/2}$ so that

$$(-1)^N \prod_{j=1}^{N} \left(1 - \frac{c}{\zeta_j^2}\right) = \prod_{j=2,4,6\ldots}^{N} \left(1 - \frac{c}{\zeta_j}\right)^2 = (1 - c^{N/2})^2$$

and therefore

$$\frac{1}{2N^2} \sum_{j=1}^{N} \log(\zeta_j F'(\zeta_j)) = \frac{1}{N^2} \log(1 - c^{N/2})$$

Please note that the evaluation of this sum can be readily generalized to the family of curves given by $F(z) = z + \frac{c}{z^{(p-1)}}$ where p is prime. Then $zF'(z) = z - \frac{(p-1)c}{z^{(p-1)}}$, and of course, as before, if $N \neq 0 \ mod \ p$, raising the N^{th} roots of unity to the p^{th} power simply reshuffles them so that

$$\frac{1}{2N^2} \sum_{j=1}^{N} \log(\zeta_j F'(\zeta_j)) = \frac{1}{2N^2} \log(1 - ((p-1)c)^N)$$

In the case that $N = 0 \ mod \ p$,

$$\prod_{j=1}^{N} \left(1 - \frac{(p-1)c}{\zeta_j^p}\right) = \prod_{j=p,2p,3p\ldots}^{N} \left(1 - \frac{(p-1)c}{\zeta_j}\right)^p = (1 - ((p-1)c)^{\frac{N}{p}})^p$$

and we conclude that

$$\frac{1}{2N^2}\sum_{j=1}^{N}\log(\zeta_j F'(\zeta_j)) = \frac{p}{2N^2}\log(1-((p-1)c)^{\frac{N}{p}}).$$

Now we just need to evaluate the second sum for the ellipse and we will have the exact energy expression for a uniform arrangement of charges. To this end we need to obtain the $u's$ which satisfy the equation $F(\zeta_j) = F(u)$ or $u^2 - uF(\zeta_j) + c = 0$. It is clear that $u = \zeta_j$ satisfies the equation, and from this it follows that, since the product of the two roots of the above quadratic is c, the other u must be $\frac{c}{\zeta_j}$.

We now have:

$$\frac{1}{2N^2}\sum_{j=1}^{N}\sum_{u\in F^{-1}\{F(v)\},u\neq v}\log(u^N - v^N) = \frac{1}{2N}\log(1-c^N)$$

since $\zeta_j^N = 1$.

Finally, for odd N,

$$E_N = -\frac{\log N}{N} - \frac{1}{2N}\log(1-c^N) + \frac{1}{2N^2}\log(1-c^N)$$

while for even N, we have:

$$E_N = -\frac{\log N}{N} - \frac{1}{2N}\log(1-c^N) + \frac{1}{N^2}\log(1-c^{\frac{N}{2}})$$

The remaining material in this chapter should be considered to be more heuristic in content.

2.4. Heuristic Discussion of Energies

We have just completed a careful analysis of the self-energy in the case in which the charges are uniformly distributed on the unit circle. Now we extend this discussion to include the effects of a non-constant charge density on the circle. In fact, if we define the charge density to be the smooth function of j defined so that

$$\theta_J - \theta_K = \int_K^J \frac{dj}{N\rho_j} \tag{18}$$

If ρ_j is independent of j we know that equation (11) gives an essentially exact answer for the large-N case.

Our result for contributions of the self-energy to the potential for a single particle is given by equation (17), which can be written in terms of the spacing between particles on the curve C which is given by a spacing factor on the circle times the conversion factor from circle it curve $1/F'$. Thus the spacing is

$$\delta = \frac{|vF'(v)|}{2N\pi\rho} \tag{19}$$

If we take our original expression for the self-energy contribution to the potential, and then say that this contribution to the real potential depends only on the actual spacing we find a potential contribution

$$\phi_s(j) = \frac{1}{N} \log\left[\frac{|F'(v_j)|}{2N\pi\rho_j}\right] \tag{20}$$

Just as before, we calculate a contribution to the total energy by taking half the potential multiplied by the charge density and adding. We find

$$E_s = \frac{1}{2N} \sum_{j=1}^{N} \log\left[\frac{|F'(v_j)|}{2N\pi\rho_j}\right] \tag{21}$$

This energy is the continuum value (zero) plus a contribution from the replacement of the line of charge distributions immediately surrounding a given charge (which is included in the continuum energy), by the self energy of the point charge which replaces it, and is not included in the energetic calculation. This is the charge in question $1/N$ times the separation of the charges on the line, $\log 1/N$. One can also write this energy as an integral over the circle of the form

$$E_s = \frac{1}{2N} \int_0^{2\pi} d\theta \ \rho(\theta) \log\left[\frac{|F'(v)|}{2N\pi\rho(\theta)}\right] \tag{22}$$

Here v is $e^{i\theta}$ and $\rho(\theta_j)$ is the same as ρ_j. This form of the energy is convenient for variational calculations.

Note the factor of one half in front of equation (22). It will be important in what follows.

The same discussion can be easily extended to the calculation of the interaction energy. Because of the logarithmic potential the result is

$$E_{corr} = \frac{1}{2}\int_0^{2\pi} d\theta\ \rho(\theta) \int_0^{2\pi} d\mu\ \rho(\mu)\ \Re\log[F(e^{i\theta}) - F(e^{i\mu})] \quad (23)$$

2.5. Variational Calculation

To construct a variational principle, we take the two energies of equations (22) and (23) add to them a Lagrange multiplier term of the form

$$-\int_0^{2\pi} d\theta\ \rho(\theta)\phi_0$$

designed to ensure that the total change is constrained to be unity. One then sets the resulting variation with respect to ρ to zero and finds

$$\phi_0 = \int_0^{2\pi} d\mu\ \rho(\mu)\ \Re\log[F(e^{i\theta}) - F(e^{i\mu})] + \frac{1}{2N}\log\left[\frac{|F'(e^{i\theta})|}{2N\pi e\rho(\theta)}\right] \quad (24)$$

The e in the last term appears as a result of varying the density inside the logarithm. Note once more the factor $1/2$ in front of the last term. This equation is as far as we can tell, new.

Equation (24) looks like the statement that the electrical potential on a conductor is constant. However, that is not quite the right interpretation. To the requisite order $(1/N)$ the right hand side of equation (24) is not the electrical potential. The electric potential is the somewhat similar expression in which the symbols e and $1/2$ just mentioned are replaced by unity, i.e.,

$$\phi(\theta) = \int_0^{2\pi} d\mu\ \rho(\mu)\ \Re\log[F(e^{i\theta}) - F(e^{i\mu})] + \frac{1}{N}\log\left[\frac{|F'(e^{i\theta})|}{2N\pi\rho(\theta)}\right]$$

This actual potential, in contrast to ϕ_0, varies in space.

In equation (24) the potential ϕ_0 can be evaluated by integrating the equation over all values of θ. The very same arguments which we used in section 2.2 to perform the integration over charges uniformly distributed on the circle can be used to simplify the expression for ϕ_0. We find

$$2\pi\phi_0 = \int_0^{2\pi} d\theta\ \frac{1}{2N}\log\left[\frac{|F'(e^{i\theta})|}{2N\pi e\rho(\theta)}\right]$$

We are looking for the lowest order terms which are of order $1/N$. Hence we can set $\rho(\theta)$ to its lowest order value $1/(2\pi)$. We can also evaluate the integral over $\log F'$ by taking the contour to infinity. In the end we find

$$2\pi\phi_0 = \int_0^{2\pi} d\theta \ \frac{1}{2N} \log\left[\frac{1}{Ne}\right]$$

so that, to order $1/N$ equation (24) becomes

$$0 = \int_0^{2\pi} d\mu \ \rho(\mu) \ \Re \log[F(e^{i\theta}) - F(e^{i\mu})] + \frac{1}{2N} \log|F'(e^{i\theta})| \qquad (25)$$

which is our desired final result.

This equation is related to the integral equation for the charge distribution in ref. 27. While our equation is a statement of the constancy of an appropriate potential on the surface of the conductor, the equation in Ref. [29] is a statement that the tangential component of the electric field is zero at each charge location, in an equilibrium configuration.

3. FOURIER SPACE ANALYSIS

We will analyze the integral equation (25) using Fourier analysis techniques. We define the Fourier coefficients of the continuum density ρ by

$$\rho_k = \int_0^{2\pi} \rho(\mu) e^{i\mu k} d\mu$$

Following Pommerenke,[28] we also define

$$s_k = \sum_{i=1}^{N} w_i^k.$$

where w_i is the location of the ith charge in the minimum energy configuration. The s_k encode information about the locations of the charges. For $k \ll N$, the s_k reflect the smooth, large scale behavior of the distribution of the charges. Thus, they should correspond to the ρ_k by

$$s_k \approx N\rho_k = N \int_0^{2\pi} \rho(\mu) e^{ik\mu} d\mu.$$

For larger k, in particular for $k \sim N$, the discreteness of the charges becomes important, and s_k will in general be very different from ρ_k.

We now rewrite the integral equation (25) in terms of these definitions. From (25) we obtain

$$\int_0^{2\pi} \rho(\mu) \Re \left[\log[e^{i\theta} - e^{i\mu}] + \log \left[\frac{F(e^{i\theta}) - F(e^{i\mu})}{e^{i\theta} - e^{i\mu}} \right] \right] d\mu$$
$$= -\Re \frac{1}{2N} \log[F'(e^{i\theta})]$$

Substituting $\rho(\mu) = \frac{1}{2\pi} \sum_k \rho_k e^{-ik\mu}$, we obtain

$$\frac{\rho_k}{k} + \sum_l a_{kl} \bar{\rho}_l = \frac{c_k}{2N},$$

where, following Pommerenke,[28] we have defined the matrix a_{kl} and the vector c_j by

$$\log \left(\frac{F(w) - F(\xi)}{w - \xi} \right) = -\sum_{k=1}^{\infty} \sum_{l=1}^{\infty} a_{kl} w^{-k} \xi^{-l},$$

and $c_j = -\sum_{k=1}^{j-1} a_{k,j-k}$, so that

$$\log F'(w) = -\sum_{k=1}^{\infty} c_k w^{-k}.$$

Solving this system of linear equations will yield the continuum density ρ. Note that the above system is only meaningful for $k = 1, 2, 3, \ldots$. We know that the total charge is 1, and this fixes $\rho_0 = 1$. We can also obtain information on the locations of the charges form the correspondence between ρ_k and s_k. For large N, using the correspondence $s_k \approx N\rho_k$, we get

$$\frac{s_k}{k} + \sum_l a_{kl} \bar{s}_l = \frac{c_k}{2}, \tag{26}$$

which is the same as the equation in Lemma 2 of ref. 28. We will henceforth refer to this as the Pommerenke equation. Note that our analysis

yields the (unexpected) conclusion that the equations determining the s_k have *no dependence* on N, the total number of charges.

We can calculate a_{kl} and c_k for the ellipse and the hypotrochoid using the explicit forms of F. In order to keep the formulae simple, and avoid the appearance of complex roots of unity, we will use the forms

$$F(\xi) = \xi + \frac{c}{\xi^r},$$

Therefore, the c in this section is the same as the c in the previous section, if we set $\xi = e^{i\pi/2} w$ for the ellipse, and $\xi = e^{i\pi} w$ for the hypotrochoid. We thus need to shift the results with our choice of mapping function by $\pi/2$ and π respectively to compare with the mapping functions in Sec. 2.

A calculation for the ellipse yields

$$a_{kl} = \frac{c^k}{k} \delta_{kl} \tag{27}$$

and

$$c_k = \begin{cases} 0 & k \text{ odd} \\ \frac{2}{k} c^{k/2} & k \text{ even} \end{cases}. \tag{28}$$

A similar calculation for the hypotrochoid shows that the energy can be put in a similar form with

$$a_{kl} = \begin{cases} 0 & k + l \neq 0 \bmod 3 \\ 0 & k < p \text{ or } l < p,\ p = (k+l)/3 \\ \frac{c^p}{p} \frac{p!}{(k-p)!(l-p)!} & \text{otherwise, } p = (k+l)/3 \end{cases} \tag{29}$$

and

$$c_k = \begin{cases} 0 & k \neq 0 \bmod 3 \\ \frac{3}{k} (2c)^{k/3} & \text{otherwise.} \end{cases} \tag{30}$$

3.1. Solving the Pommerenke Equation

For the ellipse, the matrix a_{kl} is diagonal. Consequently, Eq. (26) is easily solved to yield:

$$s_k = \begin{cases} 0 & k \text{ odd}, \\ \frac{c^{k/2}}{1+c^k} = \frac{r_0^k}{1+r_0^{2k}} & k \text{ even}. \end{cases} \tag{31}$$

which is the solution presented in.[28] Note that for this solution, s_k is real for all k. This is equivalent to the statement that there is no *symmetry breaking*. Thus this approach cannot capture the symmetry breaking for the ellipse that we see in the numerics.

This result is compared to numerical calculations in Fig. 7, which is also done with the map $F(w) = w + c/w$. The circles are the results obtained for $N = 40$, while the stars correspond to $N = 100$. As expected, the agreement is good for small enough values of c, for which the symmetry is unbroken. Moreover the agreement is better for $N = 100$ than for $N = 40$. This is in agreement with the expectation that deviation of the solution (31) from the true s_k is $O(k^2/N)$.[28]

We will now consider the hypotrochoid. We first enumerate the consequences of the three-fold symmetry as well as the reflection symmetry of the hypotrochoid. We get,

1. $s_k = 0$ for $k \neq 0 \bmod 3$ is a reflection of the symmetry of the underlying hypotrochoid under rotations by $2\pi/3$. This symmetry is

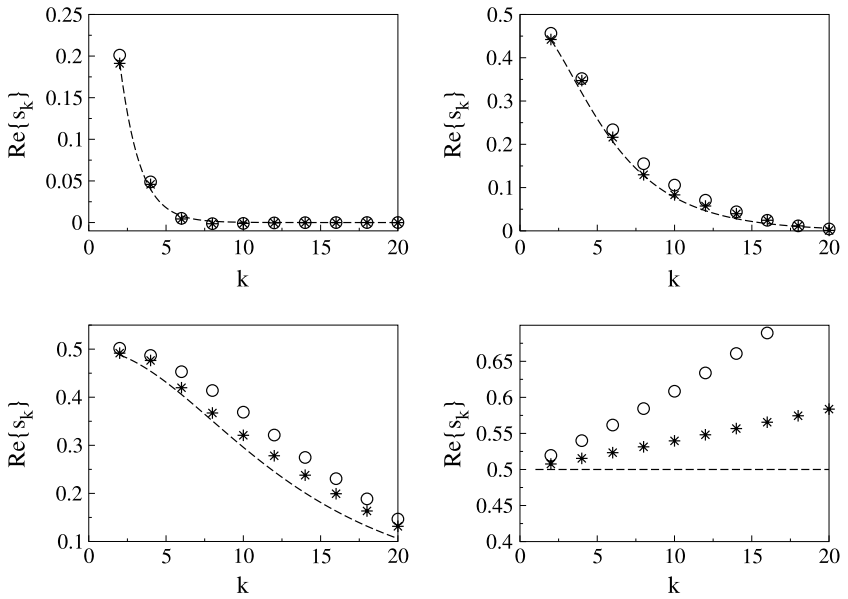

Fig. 7. s_k as a function of k for the ellipse, for c=0.2, 0.6, 0.8 and 1 respectively; the circles are the numerics obtained with $N = 40$, the stars with $N = 100$, while the dashed line is expression 31. As expected the agreement is good for small values of c, when the symmetry is preserved. The deviations are therefore stronger for $N = 40$ than for $N = 100$.

preserved in our numerically obtained solutions if the number of charges N is a multiple of 3, and is broken otherwise.

2. s_k is real as a consequence of the symmetry of the hypotrochoid under reflections about the real axis. This symmetry is broken in our numerical solutions for any N, provided that c is sufficiently close to 1/2.

If there is a unique minimizing configuration for the electrostatic energy of the hypotrochoid, the symmetries of the problem imply that $s_k = 0$ if $k \neq 0 \bmod 3$ and s_k is real for all k. These features are also reflected in the (approximate) s_k obtained by solving the Pommerenke equation. Since the Pommerenke equation is independent of N, we cannot investigate the N dependent features, like symmetry breaking for the hypotrochoid, using this approach.

We will now solve the Pommerenke equation for the hypotrochoid. If $c < 1/2$, c_k and the a_{kl} decay exponentially as k and l get large. Therefore, it is reasonable to try the series solution

$$s_k = \frac{kc_k}{2} - \sum_l (ka_{kl})\frac{l\bar{c}_l}{2} + \sum_j \sum_l (ka_{kl})(la_{lj})\frac{j\bar{c}_j}{2} + \dots .$$

This series converges (not just for the hypotrochoid, but for any admissible a_{kl}), as proved by Pommerenke.[28]

Let $s_k^{(i)}$ denote the i-th term in the series, so that

$$\begin{aligned} s_k^{(1)} &= \frac{kc_k}{2} \\ s_k^{(i+1)} &= -\sum_l ka_{kl}\bar{s}_l^{(i)}, \qquad i = 2, 3, \dots \end{aligned}$$

Eqs. (29) and (30) together give

$$\begin{aligned} s_k^{(1)} &= 0, \quad k \neq 0 \bmod 3 \\ s_{3p}^{(1)} &= \frac{3}{2}(2c)^p = \frac{3}{2}r_0^{3p} \\ s_k^{(i+1)} &= -\sum_{p=\left[\frac{k+1}{2}\right]}^{k} \left(\frac{kc^p}{p}\right) \frac{p!}{(k-p)!(2p-k)!}\bar{s}_{3p-k}^{(i)}, \quad i = 1, 2, 3, \dots \end{aligned} \tag{32}$$

Since $3p - k \neq 0 \bmod 3$ unless $k = 0 \bmod 3$, it follows that $s_k^{(i)} = 0$ if $k \neq 0 \bmod 3$ for all i. Setting $k = 3m$, $p = m + n$ and replacing the sum over

p by a sum over $n = p - m$, we get

$$s_{3m}^{(i+1)} = -\sum_{n=\left[\frac{m+1}{2}\right]}^{2m} \left(\frac{3m}{m+n}\right) \frac{(m+n)!}{(2m-n)!(2n-m)!} \left(\frac{r_0^3}{2}\right)^{m+n} \bar{s}_{3n}^{(i)}$$

$$i = 1, 2, 3, \ldots$$

$$= -3\left(\frac{r_0^3}{2}\right)^m \sum_{n=\left[\frac{m+1}{2}\right]}^{2m} \left(\frac{m}{n+m}\right)\binom{m+n}{2m-n}\left(\frac{r_0^3}{2}\right)^n \bar{s}_{3n}^{(i)}.$$

We can evaluate these sums using the saddle point method. Using Lemma 1 in Appendix A, and $s_{3m}^{(1)} = \frac{3}{2} r_0^{3m}$, we obtain the asymptotic expressions

$$s_{3m}^{(i)} \sim (-1)^i \frac{3\beta_i^m}{2}, \quad i = 1, 2, 3, \ldots$$

where

$$\beta_1 = r_0^3$$

$$\beta_{i+1} = \frac{\left[(r_0^3\beta_i + \sqrt{8r_0^3\beta_i + r_0^6\beta_i^2})\right]^3}{64\beta_i}, \quad i = 1, 2, 3, \ldots$$

and all corrections to this asymptotic result are $O(1/m)$.

At the critical parameter value $c = \frac{1}{2}$, $r_0 = 1$. In this case, $\beta_1 = 1$ and

$$\beta_{i+1} = \frac{\left[(\beta_i + \sqrt{8\beta_i + \beta_i^2})\right]^3}{64\beta_i}$$

implies that $\beta_i = 1$ for all i. Thus, the series solution breaks down in the critical case, as the solutions $s_k^{(i)}$ do not decay with i.

For parameter values close to the critical value, $c = \frac{1}{2}e^{-\epsilon}$, we have

$$r_0^3 = 2c = e^{-\epsilon} \approx 1 - \epsilon$$

If ϵ is sufficiently small, then we have β_i is close to one for the first few values of i. We can study the dependence of β_i on the parameter ϵ by setting $\beta_i = e^{-t_i\epsilon + O(\epsilon^2)} = 1 - t_i\epsilon + O(\epsilon^2)$. Linearizing the relation between β_{i+1} and β_i close to the fixed point $\beta = 1, r_0 = 1$, we get

$$\beta_{i+1} = 1 - (t_i + 2)\epsilon + O(\epsilon^2) + \ldots$$

This gives

$$t_{i+1} = t_i + 2.$$

Combining this with $t_1 = 1$, we get

$$t_i = (2i - 1)$$

It is clear that this analysis is valid long as $t_i \epsilon \ll 1$, *i.e.*, for $i \lesssim \epsilon^{-1}$. Beyond this value, we can show that the β_i decay rapidly. Using this expression for the β_i, we can re-sum the series solution for s_k to obtain

$$s_{3m} = \frac{3}{2} \frac{r_0^{3m}}{1 + r_0^{6m}} + O\left(\frac{1}{m}\right).$$

The complete solution is

$$s_k = \begin{cases} 0 & k \neq 0 \bmod 3, \\ \frac{3}{2} \frac{(2c)^{k/3}}{1+(2c)^{2k/3}} (1 + O(k^{-1})) \approx \frac{3}{2} \frac{r_0^k}{1+r_0^{2k}} & k = 0 \bmod 3. \end{cases} \tag{33}$$

Note the similarity with the solution in Eq. (31). The agreement of result (33) with numerics is tested in Fig. 8. We use the map $F(w) = w - c/w^2$, but the quantities plotted are $(-1)^k s_k$, which is the same as using the map $F(w) = w + c/w^2$. For small c and for $k \ll N$, the agreement is very good. However, the agreement is rather poor if $c \sim 1/2$, indicating that the integral equation is no longer valid as we approach the singular limit $c \to 1/2$.

3.2. The Minimum Energy Configuration of the Charges

Our goal is to find the locations of the N charges on the ellipse and hypotrochoid that minimize the electrostatic energy E_N. The results from the previous section tell us that the locations w_i on the unit circle that give the appropriate locations on the ellipse and hypotrochoid by $z_i = F(w_i)$ are such that

$$\sum_{i=1}^{n} w_i^k \approx \begin{cases} \frac{r_0^k}{1+r_0^{2k}} & k \text{ even, on ellipse.} \\ \frac{3}{2} \frac{r_0^k}{1+r_0^{2k}} + O\left(\frac{1}{k}\right) & k = 0 \bmod 3, \text{ on hypotrochoid.} \\ 0 & \text{otherwise} \end{cases} \tag{34}$$

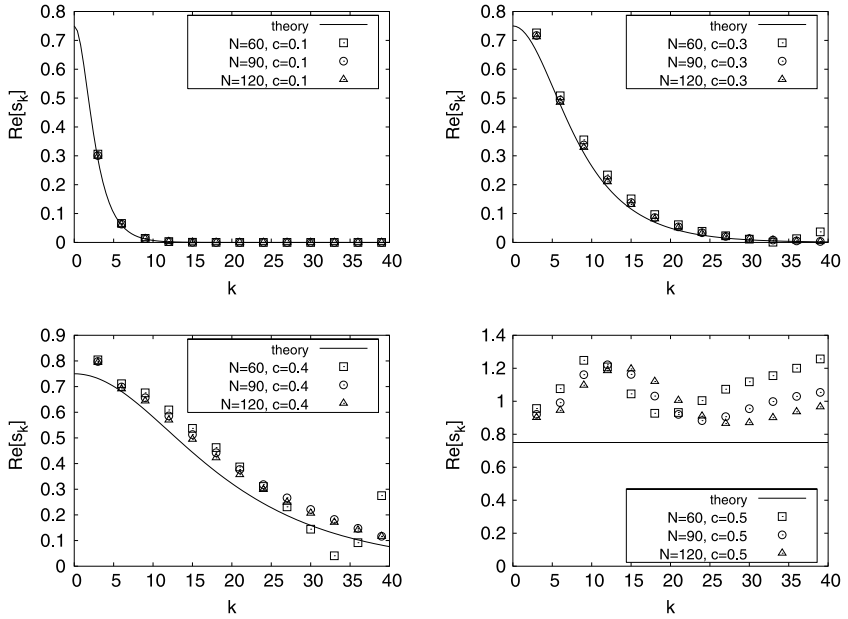

Fig. 8. s_k as a function of k for the hypotrochoid, for c=0.1, 0.3, 0.4 and 0.5 respectively. As expected the agreement is good for small values of c, when the symmetry is preserved.

for $1 \leqslant k \ll N$. The problem of finding the locations w_i reduces to the problem of solving the above set of equations.

As Pommerenke shows in ref. 28, the locations of the charges are given in terms of the solution s_k to the Pommerenke equation by

$$\theta_j \approx \theta_0 + \frac{2\pi j}{N} + \frac{1}{N}\left[\psi\left(\theta_0 + \frac{2\pi j}{N}\right) - \psi(\theta_0)\right] \tag{35}$$

where

$$\psi(\theta) = i\sum_{k=1}^{\infty}\left[\frac{s_k}{k}e^{-ik\theta} - \frac{\bar{s}_k}{k}e^{ik\theta}\right]$$

and θ_0 is an initial angle that is not determined by this analysis.

For the ellipse and the hypotrochoid, we get the series

$$\psi(\theta) = -\sum_{k=1}^{\infty}\frac{1}{k}\frac{q^k}{1+q^{2k}}\sin(mk\theta),$$

where $m=2,3$ for the ellipse and hypotrochoid respectively, and $q=r_0^m$. This series can be summed using the formula

$$\mathrm{am}(u)=\frac{\pi u}{2K}+2\sum_{n=1}^{\infty}\frac{1}{n}\frac{q^n}{1+q^{2n}}\sin\frac{n\pi u}{K}.$$

(See p. 277, Ryshik and Gradstein[16]) to yield

$$\psi(\theta)=\frac{m\theta}{4}-\frac{1}{2}\mathrm{am}\left(\frac{mK\theta}{\pi}\right).$$

$K=K(k)$ is the complete Jacobi elliptic function of the first kind[39], and the modulus k is determined by requiring that q be the nome[1],

$$q=\exp\left[-\frac{\pi K'(k)}{K(k)}\right],$$

where $K'(k)$ is the complementary complete elliptic function of the first kind, $K'(k)=K(\sqrt{1-k^2})$.

We are particularly interested in situations close to the critical value of c. In this case, $q=e^{-\epsilon}\approx 1-\epsilon$ is close to 1. From this, we infer that $K'/K\approx 0$, *i.e* k is close to 1. We will now work out the asymptotics close to $k=1, q=1$.

If $k=1-\delta$, $k^2\approx 1-2\delta$ and $k'=\sqrt{1-k^2}\sim\sqrt{2\delta}$, and we have

$$\begin{aligned}K(k)&=\int_0^{\pi/2}\frac{dx}{\sqrt{1-k^2\sin^2 x}}\\&=\int_0^{\pi/2}\frac{dx}{\sqrt{2\delta+\cos^2(x)}}+\xi(\delta)\\&=-\frac{1}{\sqrt{2}}\log(\delta)+\xi'(\delta)\end{aligned}$$

where we have extracted the dominant singularity of the integral in the second line, and ξ,ξ' are functions that remain bounded as $\delta\to 0$. We also have

$$K'\sim\int_0^{\pi/2}\frac{dx}{\sqrt{1-2\delta\sin^2 x}}=\frac{\pi}{2}+O(\delta).$$

Combining this with the previous result, and the definition of the nome q, we see that

$$q \approx \exp\left[\frac{\pi^2}{\sqrt{2}\log(\delta)}\right].$$

Rearranging this gives the result

$$\frac{\pi^2}{\sqrt{2}} - \log(q)\log(\delta) \to 0 \quad \text{as } \delta \to 0.$$

Using $\log(q) = -\epsilon$, we see that $\delta \sim \exp[-\pi^2/(\sqrt{2}\epsilon)]$, so that $K \sim -\log\delta/\sqrt{2} \sim \pi^2/(2\epsilon)$.

Fig. 9 is a comparison between the results of this calculation, and the numerically observed displacements of the charges from the positions that would correspond to a uniform distribution on the circle. The normalized deviation function

$$\psi(\theta) = \frac{m\theta}{4} - \frac{1}{2}\mathrm{am}\left(\frac{mK\theta}{\pi}\right). \tag{36}$$

corresponds to the following two changes relative to the uniform distribution on the unit circle –

1. The "charge" density in the smooth regions is increased by an amount $\delta\rho/\rho = m/(4N)$.

2. The charge moves away from the vicinity of the cusps, and this depletion region has a width $\pi/(mK) \sim 2\epsilon/(m\pi)$ around the the angles corresponding to the cusps.

Note that Figs. 9 (b), (c) and (d) are obtained with the mapping $F(w) = w - c/w^2$ and the solid lines are therefore given by the "shifted" function $\psi(\theta + \pi)$.

4. THE SINGULAR LIMIT

In this section, we investigate various aspects of the Coulomb problem on domains that are either singular, *i.e.*, have cusps or corners, or are close to being singular. We begin by first describing some of the numerical observations, which motivate the theoretical analysis that follows.

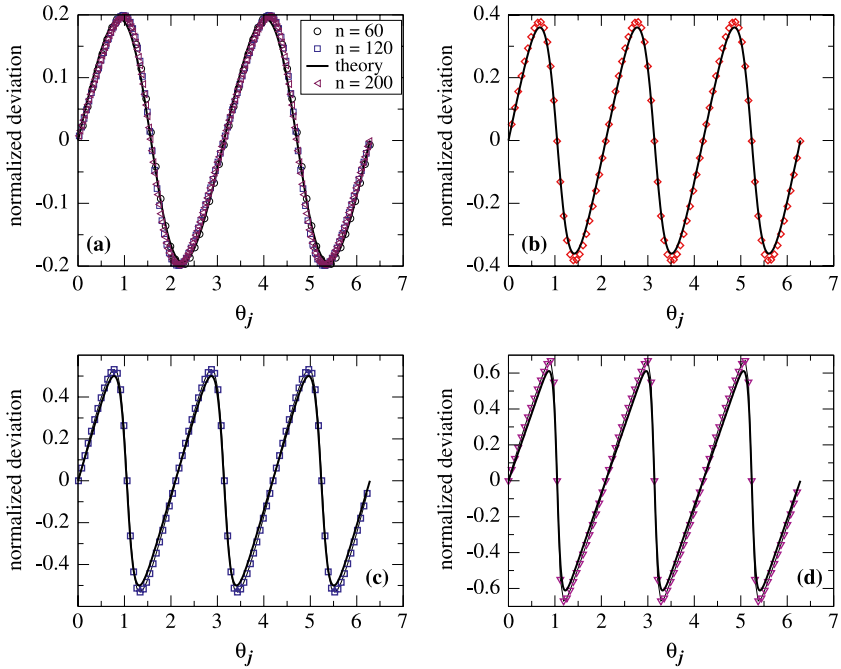

Fig. 9. A comparison between the theoretical prediction and the actual locations of the charges in the minimum energy configuration. The normalized deviation from the nominal position $\theta_j = 2\pi j/N$ is plotted. (a) shows the deviations for an ellipse with $c = 0.2$. (b), (c) and (d) depict the charge placement on a hypotrochoid with $c = 0.2, 0.3$ and 0.4 respectively. The solid lines are the theoretical prediction.

4.1. Ellipse, Hypotrochoid and Related Curves

4.1.1. Symmetry Breaking

As previously mentioned, an interesting feature of the charge placement on the ellipse and on the hypotrochoid is that the minimum energy configurations break the symmetry of the problem in certain ranges of c and N. For a given number of charges N, if the value of the parameter c is larger than a given threshold c^* which depends on N, the mirror symmetry is broken around each pointy region. The larger N, the closer the threshold is to the critical value, *i.e*, $c^*(N) \to 1$ for the ellipse and $c^*(N) \to \frac{1}{2}$ for the hypotrochoid as $N \to \infty$.

This transition can be described by a phase diagram where c^* is plotted versus N: the case of the ellipse is presented in Fig. 10 and the case of the hypotrochoid in Fig. 11.

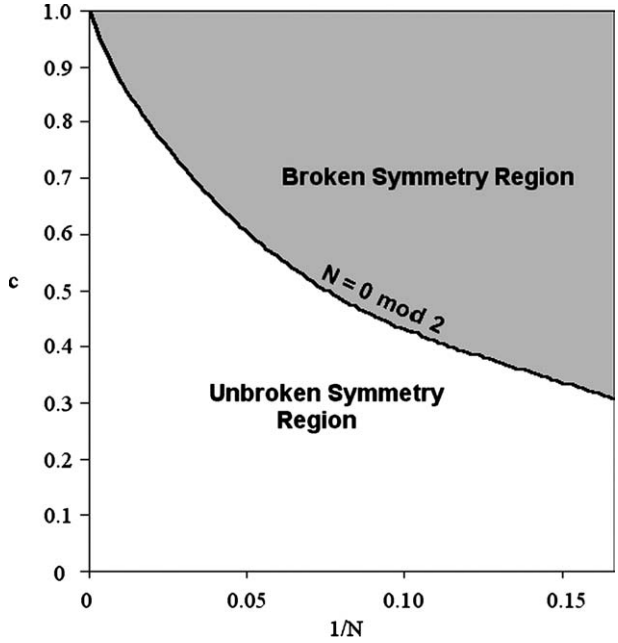

Fig. 10. Phase diagram for the ellipse.

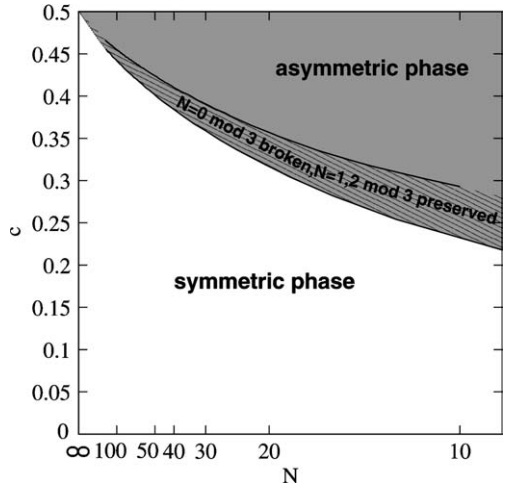

Fig. 11. Phase diagram for the hypotrochoid.

On both phase diagrams, two different cases should be distinguished, depending on the number of charges N. Let us first consider the case of the ellipse. If N is even, in the unbroken symmetry phase, the charge configuration will be symmetric versus both the vertical and the horizontal axis. Both symmetries break when $c > c^*$ (see Figure 1). On the contrary, for odd N, there is no symmetry across the long axis, while there is always symmetry across the short axis (see Figure 12). In this case, there is no transition of any sort. The value c^* at which the symmetry breaks for even N forms a curve (see Figure 10).

Similarly, in the case of the hypotrochoid, the case $N = 0 \bmod 3$ has to be distinguished from the case $N \neq 0 \bmod 3$. In the first case, a symmetric charge configuration respects the three mirror symmetries, one at each pointy region (see Figure 2). In the case $N \neq 0 \bmod 3$, only 2 out of the 3 branches of the hypotrochoid are identical, with one charge more or less than the third branch. Therefore, only one mirror symmetry is respected in this case (see Figure 13). The boundary between the broken and the unbroken symmetry phases is different for $N = 0 \bmod 3$ and for $N \neq 0 \bmod 3$ (see Figure 11).

4.1.2. Energy Dependence on N

- Line segment: As pointed out previously, a useful quantity to characterize the placement of charges on a given curve is the energy as a function of the number of charges. The case of the line segment $\Gamma_2 = [-2, 2]$ has been treated analytically in literature[27]. The energy dependence on N is given by

$$E_\Gamma^N = -\frac{\ln N}{2N} - \frac{\ln 2}{2N} - \frac{\ln N}{8N^2} - \frac{A}{2N^2},$$

where A is a constant. The first term is the self-energy. The first correction, or correlation energy, goes as N^{-s} with $s = 1$ in this case.
Other curves presenting this kind of N-dependence for the correlation energy are the star shape curves defined by the conformal mapping $F(w) = z(1 + cw^{-m})^{2/m}$[27], with $c = 1$, where $w = e^{i\theta}$ is on the unit circle and m is the number of star branches. Figure 14 shows the case $m = 3$. The dependence of the correlation energy on N is shown in Fig. 15. addition Notice that the charges are grouped near the points and that the density is lower at the center.

- Ellipse: The line segment Γ_2 is the singular limit, $c = 1$, of the ellipse defined by the conformal map $F(w) = w - \frac{c}{w}$. For a smooth curve, $c < 1$, the correlation energy goes as N^{-s} with $s = 2$ (see Fig. 16).

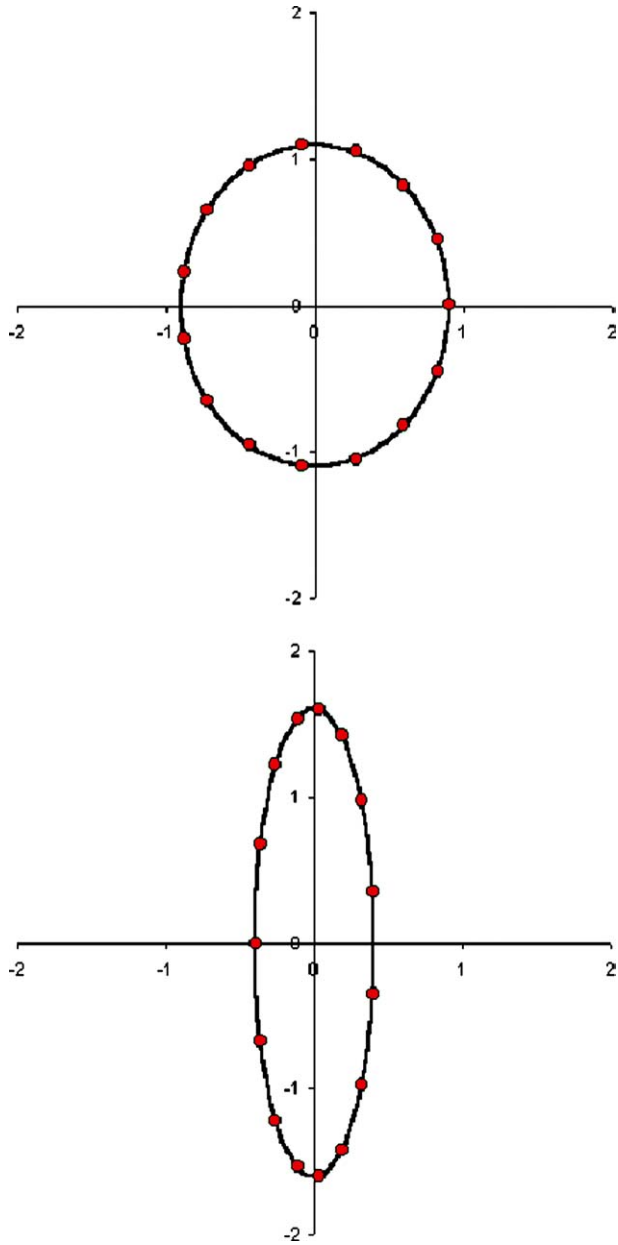

Fig. 12. Placement of 15 charges on two different ellipses, $c = 0.1$ and $c = 0.7$ respectively. Notice the breaking of the parity symmetry in part b.

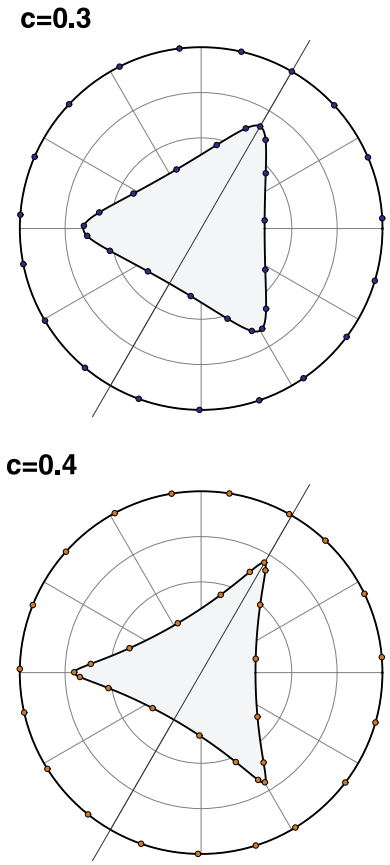

Fig. 13. Placement of 19 charges on two different hypotrochoids, $c = 0.3$ and $c = 0.4$ respectively. Notice the breaking of the parity symmetry in part b.

See the work of Pommerenke[28] where it is shown that s = 2 for any smooth curve. In the case c close to but smaller than 1, we observe a crossover as a function of the number of charges N: for smaller values of N, $s = 1$, while for larger values of N, $s = 2$, as shown in Fig. 16.
The same N dependences are observed for the star shape curves for $0 < c < 1$ (see Fig. 17). The different situations are depicted in Fig. 18.

- Hypotrochoid: In its singular limit, $c = 0.5$, the hypotrochoid has a correlation energy of the form N^{-s} with $s = 1.5$ according to the theory described below. The data supports this result (see Fig. 3), whereas $s =$

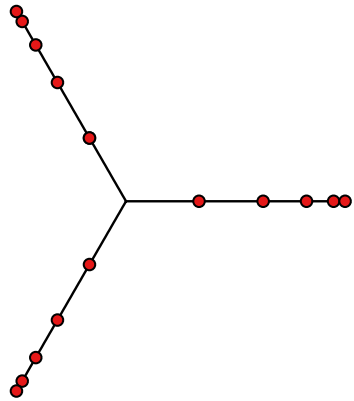

Fig. 14. Placement of 15 charges on a star shape curve with 3 branches for $c=1$.

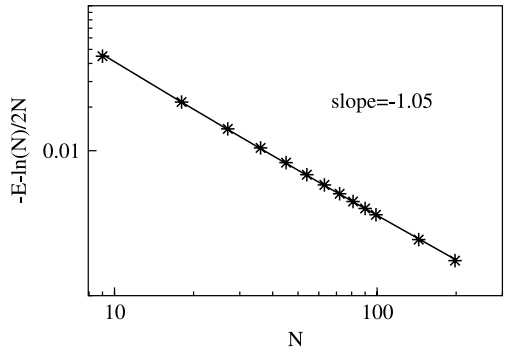

Fig. 15. Dependence of the correlation energy on N for the star shape curve with 3 branches. The slope shown for the data is consistent with the value -1.0.

2 for smooth cases $c < 0.5$. As for the previous curves, a crossover is observed from $s=1.5$ for smaller N to $s=2$ for larger N when c is close to but smaller than 0.5 (see Fig. 3).

4.2. Regular Polygons

4.2.1. Schwarz-Christoffel Map

Another kind of domains we have been interested in are regular polygons. The conformal map applying the interior of the unit circle into the interior of a given polygon is known as the Schwarz-Christoffel

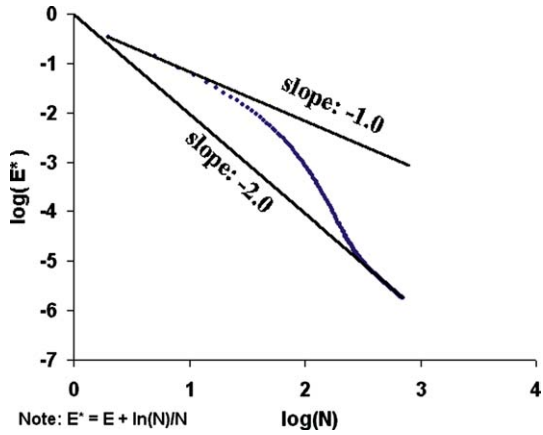

Fig. 16. Dependence of the correlation energy on N for the ellipse, with $c = 0.975$.

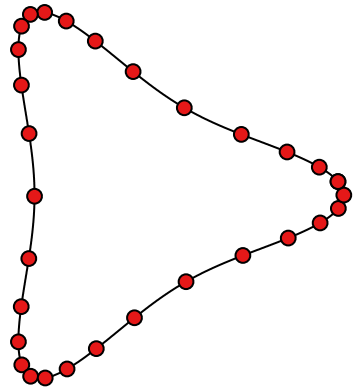

Fig. 17. Placement of 30 charges on a star shape curve with 3 branches, with $c = 0.5$.

transformation[10] given by

$$F(w) = F(w_0) + c\int_{w_0}^{w} \prod_{j=1}^{n} (1 - \zeta/w_j)^{\alpha_j - 1} d\zeta \tag{37}$$

where w_j are the pre-images of the vertices on the unit circle, $\alpha_j \pi$ are the interior angles at the vertices and w_0 and c are complex constants. A variation of Eq. 37 is the map applying the interior of the unit circle onto the

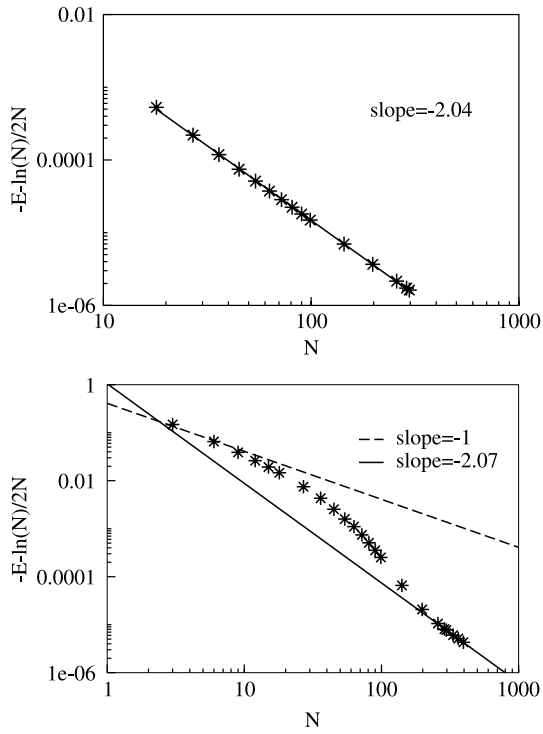

Fig. 18. Dependence of the correlation energy on N for the star shape curve with 3 branches, for $c = 0.5$ and $c = 0.95$. The slopes of the line is consistent with the theoretical values of -1.0 and -2.0.

exterior of a polygon, given by[10]

$$F(w) = F(w_0) + c \int_{w_0}^{w} \zeta^{-2} \prod_{j=1}^{n} (1 - \zeta / w_j)^{\alpha_j - 1} d\zeta. \tag{38}$$

Finally, the map we are interested in which takes the exterior of the unit circle into the exterior of the polygon is obtained by replacing w by $1/w$ in Eq. 38.

In order to compute these maps, we have used the FORTRAN package SCPACK developed by L. N. Trefethen,[37] as well as the MATLAB SC Toolbox developed by T. A. Driscoll.[10]

Let us remark that in order to fullfil the condition $F(w) \to w$ as $w \to \infty$, we need to choose the size of our regular polygons properly.

4.2.2. Symmetry Breaking

As for the other curves considered, we observe a symmetry breaking of the placement of charges on regular polygons. However, the process is slightly different from the one observed for the hypotrochoid or the ellipse. Indeed, for both these curves, in the singular limit, the symmetry is broken for any finite value of N. Regular polygons do not present cusps, but corners. Depending on the value of the interior angles, the symmetry breaks only for N larger than a threshold value N^*. For small enough values of N, the charges remain far enough from the corners to be unaffected by the charges sitting on the other sides of the polygon. When N increases, the charges closest to the corner slightly shift to avoid being just in front of the charges on the neighboring side. This effect is much more pronounced on curves presenting cusps, because the distance between charges placed on two neighboring branches decreases much faster as one approaches the cusp. Therefore, the symmetry breaks for any finite N.

Figure 19 shows the placement of 6 charges on an equilateral triangle and of 8 charges on a square. Due to the small value of the interior angles in the case of the triangle, the symmetry is broken, while it is preserved for the square.

4.2.3. Minimum Energy Configuration

In order to characterize the minimum energy configuration, we have computed the deviation function $\psi(\theta)$ for the regular hexagon, for different values of N. The results are presented in Fig. 20. The charges sitting at the corners remain unshifted, while the ones sitting on one side of the hexagon shift toward the closest corner. If the number of charges on one

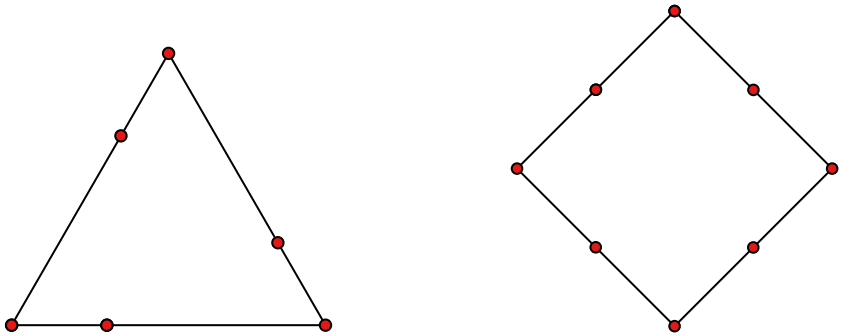

Fig. 19. Placement of 6 charges on an equilateral triangle and of 8 charges on a square; the symmetry is broken in the first case and preserved in the second.

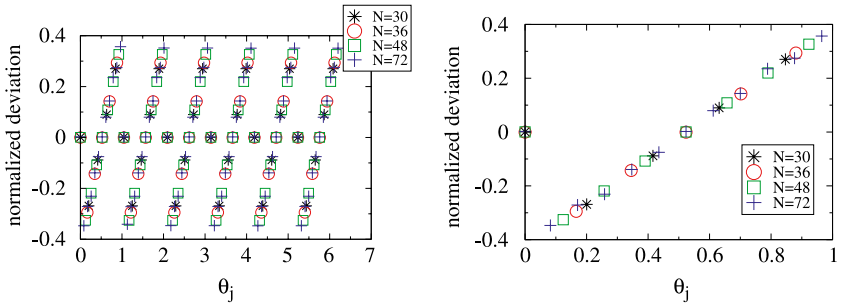

Fig. 20. Deviation function ψ for the regular hexagon.

side is odd (like for $N=30$, $N=36$, $N=48$ and $N=72$), the central charge does not shift.

For regular polygons, the correlation energy depends on N as N^{-s} with $s=2$ according to the theory described below. Figures 21 and 22 show this dependence for a regular hexagon and a regular octagon.

4.3. Scaling Arguments for the Energy Dependence

The different dependences of the energy on the number of charges N can be easily understood.

The energy itself is of order unity for a two-dimensional conductor of arbitrary size. There are N^2 interactions, each of strength $1/N^2$. The size is picked so that this leading order term in the correlation energy is zero for when the charges are in their unshifted position. The shift in position for each particle is of order $1/N$ and all the particles and interactions

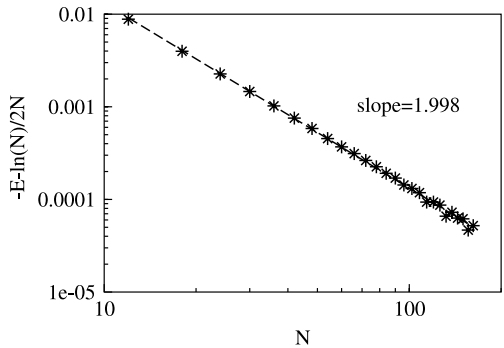

Fig. 21. Dependence of the correlation energy on N for the regular hexagon.

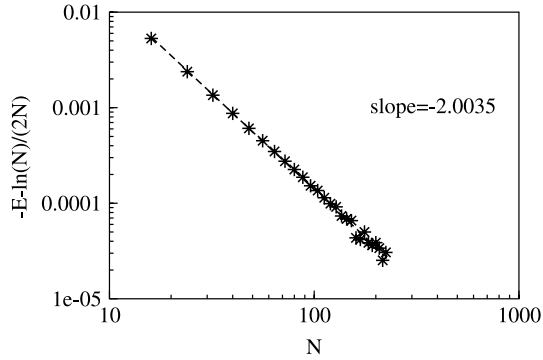

Fig. 22. Dependence of the correlation energy on N for the regular octagon.

participate roughly equally in the shift. Since the energy obeys a variational principle, the energy varies as the square of the shift, or as $1/N^2$.

To find the shift in the singular case, consider first a simplified model in which charges appear in two concentric closely spaced circles. To make all the important distances comparable take the spacing between the circles to be the same as the spacing between the charges in each circle, i.e. $2\pi/N$. Compare two cases, one with the charges lined up (see Fig. 23); the other with the inner circle rotated so that no two charges are very close to one another (see Fig. 24). In the second case, the distance between the closest charges has increased roughly by a factor of two. These closest interactions, each of order $1/N^2$ have changed by an additive term

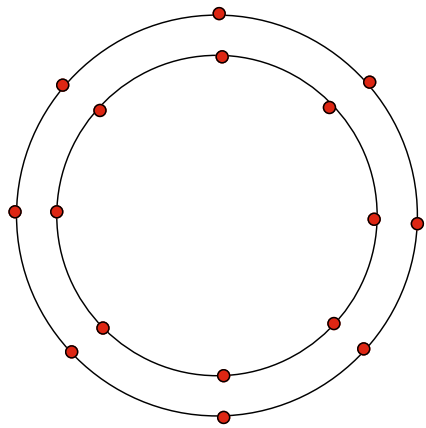

Fig. 23. Two concentric circles, with the charges lined up.

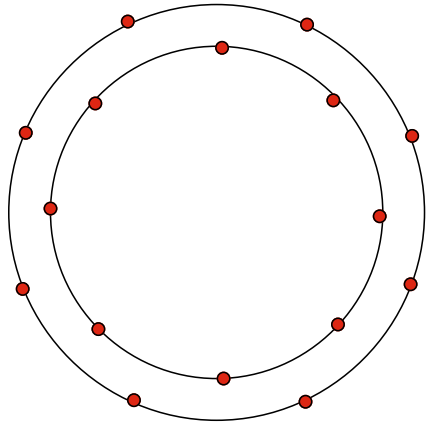

Fig. 24. Two concentric circles, shifted.

of order $(1/N^2)\ln 2$. Thus the entire change in correlation energy is of order $1/N$.

The very same argument applies to the hypotrochoid, except in that it applies to only some of the charges. Look at the small distance s from the point of the hypotrochoid. There are, once gain, two almost parallel lines. At a distance s we have a number of charges, J, given by $(J/N)^2 \sim s$ and a separation between the two lines given by $\delta \sim (j/N)^3$. The separation between two changes on a single branch is the J derivative of $(J/N)^2$ or $\sim J/N^2$. The number of charges sensitive to the distortion effects are the ones with δ less than or of the order of this separation. Hence we have

$$(J/N)^3 \sim (J/N)(1/N)$$

or a number of particle $J \sim N^{1/2}$ whose interaction with the nearest neighboring charges can be changed by an amount of order unity. These particles each have an interaction of order $1/N^2$, so that the total change is $1/N^{3/2}$, as observed numerically.

For the very skinny ellipse, or for the line segment, all the particles participate, as happens with the concentric circles, so that the change is of order $1/N$.

For a polygon, only the very few particles nearest to the corner participate. Hence the singular change in the energy is of order $1/N^2$.

The crossover observed for values of c close to but smaller than c^* can be understood as follows. For a sufficiently small number of charges, the charges behave as if the curve were singular: the symmetry is broken

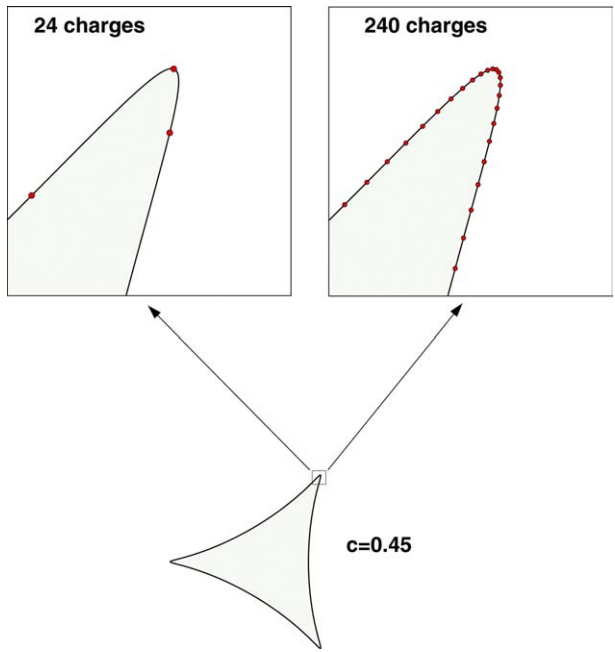

Fig. 25. Charge placement for the hypotrochoid with $c = 0.45$, for 24 and 240 charges.

and the above arguments apply. But when N increases, the smoothness of the curve prevails, the symmetry is restored and the correlation energy goes as N^{-s} with $s = 2$. This is illustrated in Fig. 25, where the placement of charges near a cusp is shown for the hypotrochoid with $c = 0.45$, for $N = 24$ and $N = 240$.

4.4. Symmetry Breaking

We can also estimate the energy of the symmetric placement of the charges (See Appendix B). By considering a test (possibly non-optimal) *uniform symmetric configuration* $w_j = \exp(2\pi i j/N + i\theta_0)$, we see that, with appropriate choices of θ_0, the minimum energy symmetric configuration for an ellipse has an energy

$$E_n \simeq -\frac{\log N}{2N} - \begin{cases} \frac{1}{2}\left[N^{-1} - N^{-2}\right]\log(1 - e^{-N\epsilon}) & N \text{ odd}, \\ N^{-2}\log(1 - e^{-N\epsilon/2}) + N^{-1}\log(1 - e^{-N\epsilon}) & N \text{ even}, \end{cases}$$

For the hypotrochoid, we have

$$E_n \simeq -\frac{\log N}{2N} - \begin{cases} CN^{-2}e^{-N\epsilon} & N \neq 0 \bmod 3, \\ C'N^{-2}e^{-N\epsilon/3} + C''N^{-2}e^{-N\epsilon} & N = 0 \bmod 3, \end{cases}$$

where we expect that, for an appropriate θ_0, the constants C, C', C'' are all positive (See Appendix 5). For $N \gg 1$ and $\epsilon > 0$,

$$-\log(1-e^{-N\epsilon/2}) \gg -\log(1-e^{-N\epsilon}), \qquad e^{-N\epsilon/3} \gg e^{-N\epsilon}.$$

Consequently, if N is odd, rather than distributing the charges uniformly on the ellipse, a "lower" energy symmetric state would correspond to having $(N-1)/2$ charges on one "branch" of the ellipse (say between $\theta = 0$ and π on the unit circle, and having $(N+1)/2$ charges on the other branch, with positions corresponding to uniform distribution of $N-1$ and $N+1$ charges respectively. For large N, the energy of such a "symmetric" state with charges at the sharp "ends" of the ellipse will be

$$E_n \simeq -\frac{\log N}{2N} + D_1 N^{-2}\log(1-e^{-N\epsilon/2}) - D_2 N^{-1}\log(1-e^{-N\epsilon}),$$

where D_1 and $D_2 > 0$ are constants that depend on whether N is even or odd. A similar argument for the hypotrochoid yields

$$E_n \simeq -\frac{\log N}{2N} - CN^{-2}e^{-N\epsilon/3},$$

with a positive constant C that depends on whether or not N is divisible by 3.

The above arguments show that, the "symmetry broken" states have

$$E_n \simeq -\frac{\log N}{2N} - \begin{cases} AN^{-1} & \text{ellipse} \\ BN^{-3/2} & \text{hypotrochoid} \end{cases}$$

with $A, B > 0$. Comparing the two expressions, we see that the crossover in the energy scaling, as well as the symmetry breaking transition occur at

$$\epsilon \sim \begin{cases} N^{-1}(1-e^{-A/D_2}) & \text{ellipse,} \\ 3N^{-1}(\frac{1}{2}\log N + F) & \text{hypotrochoid,} \end{cases}$$

where $F = \log B - \log C$.

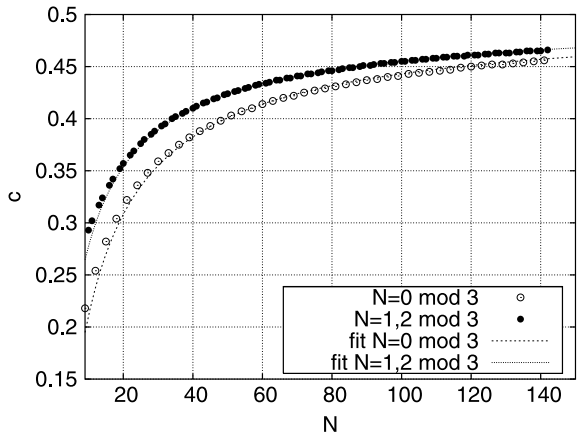

Fig. 26. A comparison between the predicted and the numerically observed symmetry breaking.

We compare the formula for the hypotrochoid with numerical observations. For the hypotrochoid, the above formula yields

$$c = \frac{1}{2}\exp\left[-\frac{3}{2}\frac{\log N}{N} + \frac{3F}{N}\right].$$

Fig. 26 is a plot of the c–value for the symmetry breaking, as a function of N, for the hypotrochoid. There is one fitting parameter, F, which can depend on whether or not N is divisible by 3.We see that the theory agrees very well with the numerics, both for $N = 0 \bmod 3$ and $N \neq 0 \bmod 3$. When $N = 0\, mod\, 3$ there are three "corners" which show a distortion from the symmetry breaking while in the other cases there is but one. Hence the former case has the most to gain from the symmetry breaking, and so we expect the asymmetry to persist down to lower values of c for that case. The data supports this expectation.

4.5. Universality in the Charge Locations for Singular Curves

We first consider the problem of the placement of N identical charges of strength $1/N$ on the line segment $\Gamma_1 = [-1, 1]$. The Fekete polynomial $f_N(x)$ for Γ_1 is given by

$$f_N(x) = \prod_j^N |x - \zeta_j|$$

where ζ_j are defined by

$$\prod_{i=1}^{N}\prod_{j\neq i}^{N}|\zeta_i-\zeta_j|=\max_{x_1,\ldots,x_N\in[-1,1]}\prod_{i=1}^{N}\prod_{j\neq i}^{N}|x_i-x_j|.$$

f_N obeys the equation[33]

$$(1-x^2)f_N''+N(N-1)f_N=0.$$

The solution can be expressed as

$$f_N(x)=c_N(x^2-1)P_{N-1}'(x)=2^N\binom{2N}{N}^{-1}\{P_N(x)-P_{N-2}(x)\},$$

where P_k denotes the Legendre polynomial of degree k[33,34,38]. N identical charges therefore place themselves at the ends of the segment and at the positions of the extrema of the Legendre polynomial of degree $N-1$, or equivalently at the intersections of the Legendre polynomials of degrees N and $N-2$. Figure 27 represents the case $N=20$. The charges accumulate toward the ends. This is consistent with the solution of the continuum problem, i.e., the equilibrium charge density on the line segment $\Gamma_1=[-1,1]$, corresponding to the situation $N\to\infty$, and given by

$$\rho(x)=\frac{1}{\pi}\frac{1}{\sqrt{1-x^2}}.$$

One way to characterize the placement of N identical charges on a line segment is to compute the ratio of two successive intervals between the charges, Δ_{i+1}/Δ_i where $\Delta_i=|x_{i+1}-x_i|$, $i=1$ corresponding to the charge placed at one extremity of the segment. The asymptotic dependence of Δ_{i+1}/Δ_i on N is given by

$$\Delta_{i+1}/\Delta_i=R_i-\frac{A_i}{N^2}+\mathcal{O}(N^4),$$

where R_i and A_i are two constants depending on i.

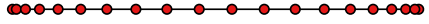

Fig. 27. Placement of 20 charges on a line segment.

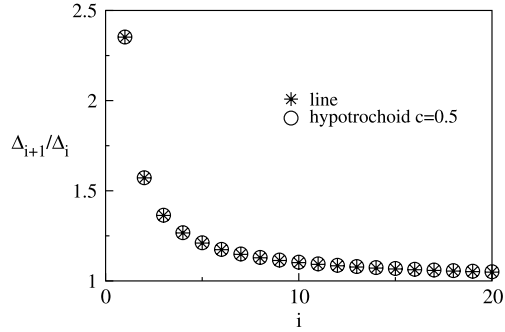

Fig. 28. Dependence of $\Delta_{i+1}/Delta_i$ on i.

The star symbols in figure 28 show the dependence of Δ_{i+1}/Δ_i on i for the line, obtained for $N=200$. As expected, Δ_{i+1}/Δ_i tends to 1 when i increases, i.e., in the central part of the line segment.

The other singular curve we are interested in is the hypotrochoid with $c=0.5$. In this singular limit, the charge symmetry is broken for any finite number of charges N. Moreover, in the limit of large N, the placement of the charges near the cusps is similar to the placement of charges on the line segment. We have projected the charges positions near one cusp on the symmetry axis of this cusp, and we have computed the quantities Δ_{i+1}/Δ_i as defined for the line segment. The results are shown in Fig. 28 by circles, computed for $N = 800$. The correspondence with the results for the line is excellent. This is a signature of universal behavior of the charge locations close to the cusp *even in the symmetry broken regime*.

Let us remark that the situation is completely different in the case of regular polygons, where we consider the placement of charges near a corner instead of a cusp. This is illustrated in Figs. 29 and 30, which show the

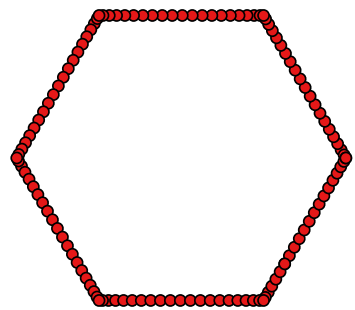

Fig. 29. Placement of 120 charges on a regular hexagon.

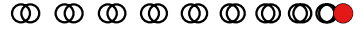

Fig. 30. Projection on the horizontal axis of the charge positions on two opposite sides of the regular hexagon of Fig. 29; the filled circle is the corner charge.

placement of 120 charges on a regular hexagon. The second figure shows the projection of the charges on the horizontal axis. The shift between two facing charges is very small, and their projections remain paired. This behavior is completely different from the one observed for the line and the hypotrochoid.

5. DISCUSSION

We have investigated some aspects of the electrostatics of discrete charges in two dimensions. The problem is of significant interest because of its connections to approximation theory,[23,9] constructing conformal maps[30] and Integrable systems.[40,25]

A dynamical version of this problem is also closely related to various Laplacian growth models because of the deep connections between conformal maps and Laplacian growth.[18,12,2] The dynamics of discrete charges in two dimensions, when they are confined by appropriate potentials,[19] is therefore relevant to electronic droplets in Quantum-Hall systems,[2] and to Laplacian growth problems including Hele-Shaw[12] and DLA.[18] The rich structure of the static problem certainly leads one to expect a similar richness in the associated dynamics, and we will investigate this question further.

In addition, the static problem is also a prototype for the following class of problems –

Find the "optimal" way to discretize a continuum quantity.

As stated, this discrete optimization formulation is much too general for us to say anything useful about it. Given a specific problem however, there is an appropriate continuum quantity, and an appropriate notion of optimality. Such problems arise in many places including approximation theory,[4,36] optimal transport,[15] in discretizing integrable systems,[3,26] *etc*.

As in the case of 2-D electrostatics, these discrete problems can have a much richer structure than the corresponding continuum problem. In particular, discretizing the continuum solution in an obvious manner *will not*, in general, be a good solution for the discrete problem. One explicitly needs to account for the discreteness in the formulation. As we show in Sec. 1, the locations of the discrete charges correspond to discretizing a density ρ which is *not* the continuum solution that minimizes the

electrostatic energy. Rather, the density ρ minimizes the *modified* energy, $E_s + E_{corr}$, which are given in Eqs. (22) and (23).

We can increase the "discreteness" of the problem, by making the curve more singular, or equivalently reducing the total number of charges N, for a fixed curve. As we increase the "discreteness", we get further away from the continuum solution. In particular, we have interesting, qualitatively new phenomena including *symmetry breaking*, which implies, among other things, the lack of a unique minimizing configuration. This is in sharp contrast to the continuum problem, which is *convex*, and therefore has a unique solution. Discreteness can thus introduce non-convexity into a problem whose continuum version is convex, and thereby change the problem qualitatively.[31,32]

One of the results from this paper is the universal behavior of the the charge distribution, *viz*., the ψ function in the neighborhood of cusps in the symmetric regime. This behavior comes out of minimizing the modified energy $E_s + E_{corr}$. This is no longer valid in the symmetry broken regime, as illustrated by Figs. 7, 8 and 9. Despite this, universal behavior persists even in the symmetry broken regime, as we illustrate in Fig. 28. It is interesting to understand the nature of this universality, and we will explore this further in the future.

APPENDIX A. SADDLE POINT EVALUATION OF $s_m^{(i)}$

To evaluate the successive terms $s_m^{(i)}$ in the series solution Eq. (32), we need the following result –

Lemma 1. Let α be a positive real number. Then,

$$\sum_{n=\left[\frac{m+1}{2}\right]}^{2m} \left(\frac{m}{n+m}\right)\binom{m+n}{2m-n}\alpha^n = \frac{1}{3}\beta^m\left(1+O\left(\frac{1}{m}\right)\right),$$

where

$$\beta = \frac{(\alpha+\sqrt{4\alpha+\alpha^2})^3}{8\alpha}$$

and

$$\binom{m+n}{2m-n} = \frac{(m+n)!}{(2m-n)!(2n-m)!}$$

denotes the binomial coefficient.

Proof. Setting $n = my$, replacing the sum over n by an integral with measure $m dy$, using Stirling's formula

$$p! = \sqrt{2\pi p}\left(\frac{p}{e}\right)^p \left[1 + O\left(\frac{1}{p}\right)\right],$$

we see that the sum

$$\sum_{n=\left[\frac{m+1}{2}\right]}^{2m} \left(\frac{m}{n+m}\right)\binom{m+n}{2m-n}\alpha^n$$

reduces to

$$\frac{m}{\sqrt{2\pi m}} \int_{y=1/2}^{2} \frac{\alpha^{my}}{1+y} \sqrt{\frac{1+y}{(2-y)(2y-1)}} \left[\frac{(1+y)^{(1+y)}}{(2-y)^{(2-y)}(2y-1)^{(2y-1)}}\right]^m dy$$

with an $O\left(\frac{1}{m}\right)$ relative error.

We will evaluate this integral by the saddle point method. Let $g(y)$ be defined as

$$g(y) = \log\left[\frac{\alpha^y (1+y)^{(1+y)}}{(2-y)^{(2-y)}(2y-1)^{(2y-1)}}\right],$$

so that the integral reduces to

$$I = \frac{m}{\sqrt{2\pi m}} \int_{y=1/2}^{2} \frac{e^{mg(y)}}{\sqrt{(1+y)(2-y)(2y-1)}} dy.$$

The maximum for $g(y)$ is at y^* given by

$$\log(\alpha) + \log(1+y^*) + \log(2-y^*) - 2\log(2y^*-1) = 0.$$

This yields the equation

$$\frac{\alpha(1+y^*)(2-y^*)}{(2y^*-1)^2} = 1.$$

Solving this quadratic equation, the relevant solution is

$$y^* = \frac{1}{2} + \frac{3}{2}\sqrt{\frac{\alpha}{4+\alpha}},$$

For $0 < \alpha < \infty$, we get $y^* \in (1/2, 2)$, so that the extremum lies within the range of integration.

$$\begin{aligned}\exp(g(y^*)) &= \frac{1}{\alpha}\left(\frac{2y^*-1}{2-y^*}\right)^3 = \frac{1}{\alpha}\left(\frac{2\sqrt{\alpha}}{\sqrt{4+\alpha}-\sqrt{\alpha}}\right)^3 \\ &= \frac{(\alpha+\sqrt{4\alpha+\alpha^2})^3}{8\alpha} = \beta.\end{aligned}$$

Expanding $g(y)$ about y^*, we get

$$g(y) = g(y^*) - \frac{9}{2(1+y^*)(2-y^*)(1-2y^*)}(y-y^*)^2 + O((y-y^*)^3)$$

so that the point y^* is a maximum for g. We are now in a position to apply the saddle point method, and for large m we obtain

$$I \sim \frac{1}{3}\beta^m$$

asymptotically, with $O(1/m)$ corrections. ∎

APPENDIX B. THE ENERGY OF SYMMETRIC CONFIGURATIONS FOR SINGULAR SHAPES

We estimate the energy of the symmetric configuration obtained by distributing the N charges uniformly on the unit circle, *i.e*, the points on the curve are $z_j = F(w_j) = F[e^{i(\theta_0 + 2\pi j/N)}]$. We are especially interested in situations close to the "singular" shape ($c = 1$ for the ellipse and $c = 1/2$ for the hypotrochoid). For this choice of w_j, we have

$$s_k = \sum_{j=0}^{N-1} w_j^k = \begin{cases} 0 & k \neq 0 \bmod N \\ N e^{ik\theta_0} & k = 0 \bmod N \end{cases}$$

As we show in Sec. 2, the deviation of the energy from that of a unit circle can be written as

$$\Delta E_N = \Re \int \frac{dw}{4\pi i w} \frac{w^N}{w^N - 1} \ln w F'(w).$$

Writing this expression in terms of s_k and the matrices a_{kl} and c_k, we get

$$\Delta E_N = \frac{1}{2} \sum_{k \geqslant 1} \sum_{l \geqslant 1} a_{kN,lN} e^{-i(k+l)N\theta_0} - \frac{1}{2N} \sum_{k \geqslant 1} c_{kN} e^{-ikN\theta_0}.$$

We will first evaluate this sum for the ellipse. Using the expressions for a_{kl} and c_k in Eqs. (27) and (28) respectively, we get

$$\Delta E_N^{ell} = \frac{1}{2} \sum_{q \geqslant 1} \frac{c^q}{q} \delta_{q,kN} e^{-2ikN\theta_0} - \frac{1}{2N} \sum_{q \geqslant 1} \frac{c^q}{q} \delta_{2q,kN} e^{-ikN\theta_0} \tag{39}$$

We need to do the cases N odd and N even separately.

If N is odd, $2q = kN$ implies that q is a multiple of N and k is even. Therefore $2q = kN$ implies $q = jN$ and $k = 2j$. Consequently, Eq. (39) yields

$$\Delta E_N^{ell} = \frac{1}{2N} \sum_{k \geqslant 1} \frac{[ce^{-2i\theta_0}]^{Nk}}{k} - \frac{1}{2N^2} \sum_{j \geqslant 1} \frac{[ce^{-2i\theta_0}]^{Nj}}{j}.$$

If N is even, $2q = kN$ implies that q is a multiple of $N/2$ and there are no restrictions on k. Therefore $2q = kN$ implies $q = k(N/2)$, and $k \geqslant 1$ is any natural number. Eq (39) now yields

$$\Delta E_N^{ell} = \frac{1}{2N} \sum_{k \geqslant 1} \frac{[ce^{-2i\theta_0}]^{Nk}}{k} - \frac{1}{N^2} \sum_{k \geqslant 1} \frac{[ce^{-2i\theta_0}]^{Nk/2}}{k}.$$

We can evaluate these sums using the identity

$$\sum_{k=1}^{\infty} \frac{e^{-\lambda k}}{k} = -\log(1 - e^{-\lambda}).$$

This yields the following *exact* result for the ellipse

$$\Delta E_N^{ell} = \begin{cases} \left[\frac{1}{2N^2} - \frac{1}{2N}\right] \log(1 - e^{-N(\epsilon + 2i\theta_0)}) & N \text{ odd} \\ -\frac{1}{2N} \log(1 - e^{-N(\epsilon+2i\theta_0)}) + \frac{1}{N^2} \log(1 - e^{-N(\epsilon+2i\theta_0)/2}) & N \text{ even} \end{cases}, \tag{40}$$

where, as defined earlier, $\epsilon = \log(c) \approx 1 - c$

B.1. Hypotrochoid

We can do a similar calculation for the hypotrochoid. Using the expressions in Eqs. (29) and (30), we obtain

$$\Delta E_N^{hypo} = \frac{1}{2} \sum_{q \geqslant 1} \frac{c^q}{q} \left[\sum_{p=0}^{q} \delta_{q+p,kN} \delta_{2q-p,lN} \binom{q}{p} - \frac{1}{N} 2^q \delta_{3q,jN} \right] e^{-3iq\theta_0} \tag{41}$$

We will now look which values of q and p contribute in the above summation.

$$q + p = 0, 2q - p = 0 \bmod N \quad \Longrightarrow \quad 3q = 0, 3p = 0 \bmod N.$$

We therefore need to do the cases $N = 0 \bmod 3$ and $N \neq 0 \bmod 3$ separately. If $N \neq 0 \bmod 3$, $3q = 0 \bmod N$ and $3p = 0 \bmod N$ imply that that $q = jN$, $p = mN$, where j, m are integers. In this case, Eq. (41) yields

$$\begin{aligned} \Delta E_N^{hypo} &= \frac{1}{2N} \sum_{j \geqslant 1} \frac{[ce^{-3i\theta_0}]^{jN}}{j} \left[\sum_{m=0}^{j} \binom{jN}{mN} - \frac{1}{N} 2^{jN} \right] \\ &= I + II \end{aligned} \tag{42}$$

We can estimate part II of the sum as above. We have

$$-\frac{1}{2N^2} \sum_{j \geqslant 1} \frac{[ce^{-3i\theta_0}]^{jN}}{j} 2^{jN} = \frac{1}{2N^2} \log\left[1 - [2ce^{-3i\theta_0}]^N\right]$$

To estimate part I, we use the identity

$$\sum_{\beta=0}^{N-1} \left(1 + e^{2\pi i\beta/N}\right)^{jN} = N \sum_{m=0}^{j} \binom{jN}{mN}.$$

Using this, and the above considerations, we get

$$I = \frac{1}{2N^2} \sum_{j \geqslant 1} \frac{[ce^{-3i\theta_0}]^{jN}}{j} \sum_{\beta=0}^{N-1} \left(1 + e^{2\pi i\beta/N}\right)^{jN}$$

Interchanging the order of the summations, we get

$$I = \frac{1}{2N^2} \sum_{\beta=0}^{N-1} \log\left[1 - \left[ce^{-3i\theta_0}\left(1 + e^{2\pi i\beta/N}\right)\right]^N\right]$$

Since

$$\left(1 + e^{2\pi i\beta/N}\right)^N = 2^N \cos^N\left(\frac{\pi\beta}{N}\right) e^{i\pi\beta},$$

writing $\sum_{\beta=0}^{N-1} = \sum_{\beta=-N/2}^{N/2-1}$, and using $2c = e^{-\epsilon}$ we get

$$\begin{aligned} I \ &= \frac{1}{4N^2} \sum_{\beta=N/2}^{N/2-1} \log\left[1 + e^{-2N\epsilon} \cos^{2N}\left(\frac{\pi\beta}{N}\right)\right. \\ &\qquad \left. -2(-1)^\beta e^{-N\epsilon} \cos^N\left(\frac{\pi\beta}{N}\right) \cos(3N\theta_0)\right] \end{aligned}$$

We will estimate this term for $\theta_0 = 0$. We get,

$$I = \frac{1}{2N^2} \sum_{\beta=N/2}^{N/2-1} \log\left[1 - (-1)^\beta e^{-N\epsilon} \cos^N\left(\frac{\pi\beta}{N}\right)\right].$$

We will estimate the sums over odd β and even β separately. We get

$$\begin{aligned} I = \frac{1}{2N^2} \Bigg[& \sum_{\beta \text{ odd}} \log\left[1 + e^{-N\epsilon} \cos^N\left(\frac{\pi\beta}{N}\right)\right] \\ & + \sum_{\beta \text{ even}} \log\left[1 - e^{-N\epsilon} \cos^N\left(\frac{\pi\beta}{N}\right)\right]\Bigg] \end{aligned}$$

Note that the terms with odd β are all positive, and the terms with even β are all negative.

It is easy to verify that, for an appropriate constant C, we have

$$e^{-\theta^2/2}(1-C\theta^4) \leqslant \cos(\theta) \leqslant e^{-\theta^2/2}, \qquad -\pi/2 \leqslant \theta \leqslant \pi/2.$$

Using this, for $-N/2 \leqslant \beta \leqslant N/2$, we get

$$\exp\left(-\frac{\pi^2\beta^2}{2N}\right)\left(1-\frac{C'\beta^4}{N^4}\right)^N \leqslant \cos^N\left(\frac{\pi\beta}{N}\right) \leqslant \exp\left(-\frac{\pi^2\beta^2}{2N}\right),$$

where C' is an appropriate constant. It is clear from the above inequalities, that $\cos^N\left(\frac{\pi\beta}{N}\right)$ is significantly different from zero only for $|\beta| \lesssim \sqrt{N} \ll N/2$ as $N \to \infty$. Also, if $\beta \sim O(\sqrt{N})$ we have

$$\left|1-\left(1-\frac{C'\beta^4}{N^4}\right)^N\right| \lesssim O\left(\frac{1}{N}\right)$$

in the region where the exponential $e^{-\pi^2\beta^2/2N}$ is not exponentially small. Consequently, the relative error in the approximation

$$\cos^N\left(\frac{\pi\beta}{N}\right) \approx \exp\left(-\frac{\pi^2\beta^2}{2N}\right),$$

goes to zero as $N \to \infty$. We thus obtain

$$\begin{aligned}\frac{1}{4N^2}\sum_{\beta=-N/2}^{N/2-1} \log\left[1-\alpha\cos^N\left(\frac{\pi\beta}{N}\right)\right] &\approx \frac{1}{4N^2}\int_{-N/2}^{N/2} \log\left[1-\alpha\exp\left(\frac{-\pi^2\beta^2}{2N}\right)\right] d\beta \\ &\approx \frac{1}{4\sqrt{\pi N^3}}\int_{-\infty}^{\infty} \log\left[1-\alpha\exp(-x^2/2)\right] dx,\end{aligned}$$

where we set $x = \pi\beta/\sqrt{N}$, and the relative error is $O(N^{-1})$ as $N \to \infty$.

Note also, if the sum over β was restricted to either only odd or only even β, we have to multiply the final integral by $1/2$ to obtain the right answer. This can be justified since the integrand only varies on a scale

$\beta \sim \sqrt{N} \gg 1$, so that the sum over the even β should very nearly equal the sum over the odd β.

We will now evaluate the integral in the last line for $|\alpha| \leqslant 1$. Using

$$\log(1-y) = -\left[y + \frac{y^2}{2} + \frac{y^3}{3} + \cdots \right],$$

and integrating the resulting series termwise, we get

$$\int_{-\infty}^{\infty} \log\left[1 - \alpha \exp(-x^2/2)\right] dx = -\sqrt{2\pi} \sum_{k=1}^{\infty} \frac{\alpha^k}{k^{3/2}}.$$

We define

$$G(\alpha) = \sum_{k=1}^{\infty} \frac{\alpha^k}{k^{3/2}}, \quad |\alpha| < 1.$$

It is easy to see that, at $\alpha = 1$, the sum is the Riemann zeta function $G(1) = \zeta(3/2)$. Also, the series for $G'(\alpha)$ diverges like $C/\sqrt{1-\alpha}$ as $\alpha \to 1$. Consequently, for α close to 1, we have

$$G(\alpha) = \zeta(3/2) - C\sqrt{1-\alpha} + O(|1-\alpha|^{3/2}).$$

Also, $G(0) = 0$, $G'(0) = 1$ and $G''(0) = 1/\sqrt{8}$.

Using the above considerations, we can estimate the term I as

$$I = -\frac{1}{4\sqrt{2N^3}} \left[G(e^{-N\epsilon}) + G(-e^{-N\epsilon}) \right] + O\left(\frac{e^{-N\epsilon}}{N^{5/2}} \right).$$

Therefore, we have,

$$I \approx \begin{cases} -\frac{\zeta(3/2)}{8N^{3/2}} & N\epsilon \ll 1, \\ -\frac{e^{-2N\epsilon}}{8N^{3/2}} + O\left(\frac{e^{-N\epsilon}}{N^{5/2}}\right) & N\epsilon \gg 1. \end{cases}$$

We now consider the case $N = 0 \bmod 3$. Te only terms in the summations in eq. (41) that contribute arise from

$$q + p = 0, 2q - p = 0 \bmod N \Longrightarrow 3q = 0, 3p = 0 \bmod N.$$

Since $N=0 \bmod 3$, $3q=0 \bmod N$ and $3p=0 \bmod N$ imply that $q=jL$, $p=mL$, where j,m are integers, and $L=N/3$. Also, $q+p=0 \bmod N$ implies that $j+m=0 \bmod 3$, and this also implies $2p-q=pN-(p+q)M=0 \bmod N$.

If $j=3k-r$, where $r\in\{0,1,2\}$, it follows that $m=3t+r$, where k,r are integers. Also, $q=jL=kN-rL$ and $p=mL=tN+rL$. Consequently, eq. (41) yields

$$\begin{aligned}\Delta E_N^{hypo} &= \frac{1}{2}\sum_{r=0}^{2}\sum_{k\geqslant 1}\frac{[ce^{-3i\theta_0}]^{kN-rL}}{kN-rL}\left[\sum_{t=0}^{k-[r/2]}\binom{kN-rL}{tN+rL}\right] \\ &\quad -\frac{1}{2NL}\sum_{j\geqslant 1}\frac{[2ce^{-3i\theta_0}]^{jL}}{j} \\ &= I+II \end{aligned} \tag{43}$$

Part II gives

$$-\frac{1}{2NL}\sum_{j\geqslant 1}\frac{[2ce^{-3i\theta_0}]^{jL}}{j}=\frac{3}{2N^2}\log\left[1-[2ce^{-3i\theta_0}]^{N/3}\right]$$

To estimate part I, we use the identity

$$\sum_{\beta=0}^{N-1}e^{-2\pi i\beta r/3}\left(1+e^{2\pi i\beta/N}\right)^{kN-rL}=N\sum_{t=0}^{k-[r/2]}\binom{kN-rL}{tN+rL}.$$

Using this in eq. (43), we get

$$I=\frac{1}{2N}\sum_{r=0}^{2}e^{-2\pi i\beta r/3}\sum_{k\geqslant 1}\frac{[ce^{-3i\theta_0}]^{kN-rL}}{kN-rL}\sum_{\beta=0}^{N-1}\left(1+e^{2\pi i\beta/N}\right)^{kN-rL} \tag{44}$$

For all complex number $|z|<1$ and $r=0,1,2$, we have

$$3\sum_{k\geqslant 1}\frac{z^{3k-r}}{3k-r}=\begin{cases}-\log(1-z^3), & r=0,\\ -\log(1-z)-\omega^2\log(1-\omega z)-\omega\log(1-\omega^2 z), & r=1,\\ -\log(1-z)-\omega\log(1-\omega z)-\omega^2\log(1-\omega^2 z), & r=2,\end{cases}$$

$$\sum_{k\geqslant 1}\frac{z^{3k-r}}{3k-r}=-\frac{1}{3}\sum_{s=0}^{2}\omega^{2rs}\log(1-\omega^{s}z)$$

where $\omega=e^{-2\pi i/3}$ is a cube root of unity.

Interchanging the order of the summations in (44), and using the above identities, we get

$$I=-\frac{1}{2N^2}\sum_{\beta=0}^{N-1}\sum_{s=0}^{2}\sum_{r=0}^{2}\omega^{(\beta+2s)r}\log\left[1-\omega^{s}\left[ce^{-3i\theta_0}\left(1+e^{2\pi i\beta/N}\right)\right]^{N}\right]$$

Note that

$$\sum_{r=0}^{2}\omega^{(\beta+2s)r}=\begin{cases}0 & \beta+2s\neq 0 \bmod 3\\ 3 & s=\beta \bmod 3.\end{cases}$$

Therefore,

$$I=-\frac{3}{2N^2}\sum_{\beta=0}^{N-1}\log\left[1-e^{-2\pi i\beta/3}\left[ce^{-3i\theta_0}\left(1+e^{2\pi i\beta/N}\right)\right]^{N}\right]$$

Breaking this sum up into 6 parts using β mod 6, setting $\theta_0=0$ and noticing the similarity with the $N\neq 0$ mod 3 case, we get

$$I=\frac{1}{4\sqrt{2N^3}}\sum_{r=0}^{2}\left[G(\omega^{r}e^{-N\epsilon/3})+G(-\omega^{r}e^{-N\epsilon/3})\right]+O\left(\frac{e^{-N\epsilon/3}}{N^{5/2}}\right).$$

ACKNOWLEDGMENTS

We would like to thank Paul Wiegmann, Thomas Erber, David Nelson, and Michael Brenner for helpful conversations. This research was supported by the University of Chicago MRSEC under NSF grant DMR-0213745. Additional support came from the NSF-DMR under grant 094569.

REFERENCES

1. M. Abramowitz and I. A. Stegun, editors. *Handbook of mathematical functions with formulas, graphs, and mathematical tables*. Dover Publications Inc., New York, 1992. Reprint of the 1972 edition.
2. O. Agam, E. Bettelheim, P. Wiegmann, and A. Zabrodin, Viscous fingering and the shape of an Electronic droplet in the Quantum hall regime. *Phys. Rev. Lett.* **88**:236801, (2002).
3. C. D. Ahlbrandt and A. C. Peterson, *Discrete Hamiltonian systems*, volume 16 of *Kluwer Texts in the Mathematical Sciences*. Kluwer Academic Publishers Group, Dordrecht, 1996. Difference equations, continued fractions, and Riccati equations.
4. V. V. Andrievskii and H.-P. Blatt, *Discrepancy of signed measures and polynomial approximation*. Springer Monographs in Mathematics. Springer-Verlag, New York (2002).
5. V. I. Arnold and A. Avez, editors. *Ergodic Problems of Classical Mechanics*. Benjamin, New York (1968).
6. M. Bowick, A. Cacciuto, D. Nelson, and al. Crystalline order on a sphere and the generalized Thomson problem. *Phys. Rev. Lett.* **89**:185502 (2002).
7. M. Bowick, D. Nelson, and A. Travesset, Interacting topological defects on frozen topographies. *Phys. Rev. B* **62**:8738–8751 (2000).
8. J. H. Conway and N. J. A. Sloane, *Sphere packings, lattices and groups*, volume 290 of *Grundlehren der Mathematischen Wissenschaften [Fundamental Principles of Mathematical Sciences]*. Springer-Verlag, New York, third edition, 1999. With additional contributions by E. Bannai, R. E. Borcherds, J. Leech, S. P. Norton, A. M. Odlyzko, R. A. Parker, L. Queen and B. B. Venkov.
9. P. Deift, T. Kriecherbauer, and K. T.-R. McLaughlin, New results on the equilibrium measure for logarithmic potentials in the presence of an external field. *J. Approx. Theory*, **95**(3):388–475 (1998).
10. T. A. Driscoll and L. N. Trefethen, *Schwarz-Christoffel Mapping*. Cambridge monographs on applied and computational mathematics. Cambridge University Press, Cambridge UK, 2002.
11. T. Erber and G. M. Hockney, Complex systems: equilibrium configurations of N equal charges on a sphere ($2 \leqslant N \leqslant 112$). In *Advances in chemical physics*, Vol. XCVIII, Adv. Chem. Phys., XCVIII, pages 495–594. Wiley, New York (1997).
12. M. J. Feigenbaum, I. Procaccia, and B. Davidovich, Dynamics of finger formation in Laplacian growth without surface tension. *J. Statist. Phys.* **103**(5–6):973–1007 (2001).
13. M. Fekete, über die verteilung der wurzeln bei gewissen algebraischen gleichungen mit ganzzahligen koeffizienten. *Math. Z.* **17**:228–249 (1923).
14. O. Frostman, Potentiel d'équilibre et capacité des ensembles avec quelques applications à la théorie des fonctions. *Dissertation, Lunds Univ. Mat. Sem.* **3**:1–118 1935. Dissertation.
15. W. Gangbo and R. J. McCann, The geometry of optimal transportation. *Acta Math.* **177**(2):113–161 (1996).
16. I. S. Gradstein and I. M. Ryshik, *Summen-, Produkt- und Integraltafeln. Band 1, 2*. Verlag Harri Deutsch, Thun, language edition, 1982. Translation from the Russian edited by Ludwig Boll, Based on the second German-English edition translated by Christa Berg, Lothar Berg and Martin Strauss, Incorporating the fifth Russian edition edited by Yu. V. Geronimus and M. Yu. Tseĭtlin.
17. J. M. Greene, *J. Math. Phys.* **20**:1183 (1979).
18. M. B. Hastings and L. S. Levitov, Laplacian growth as one-dimensional turbulence. *Physica D*, **116**(1–2):244–252 (1998).

19. T. L. Hughes, A. D. Klironomos, and A. T. Dorsey, Fingering of electron droplets in nonuniform magnetic fields. preprint, September 2002.
20. L. P. Kadanoff, Scaling for a critical Kolmogorov-Arnold-Moser trajectory. *Phys. Rev. Lett.* **47:**1641 (1981).
21. L. P. Kadanoff and S. J. Shenker, Critical behavior of a KAM surface: I. Empirical results. *J. Stat. Phys.* **27**:631 (1982).
22. J. Korevaar, Asymptotically neutral distributions of electrons and polynomial approximation. *Ann. of Math. (2)* **80**:403–410 (1964).
23. J. Korevaar, Fekete extreme points and related problems. In *Approximation theory and function series (Budapest, 1995)*, volume 5 of *Bolyai Soc. Math. Stud.* pages 35–62. János Bolyai Math. Soc., Budapest, 1996.
24. J. Korevaar and T. Geveci. Fields due to electrons on an analytic curve. *SIAM J. Math. Anal.* **2**:445–453 (1971).
25. I. K. Kostov, I. Krichever, M. Mineev-Weinstein, P. B. Wiegmann, and A. Zabrodin, The τ-function for analytic curves. In *Random Matrix Models and Their Applications*, Vol. 40 of *Math. Sci. Res. Inst. Publ.*, 285–299. Cambridge Univ. Press, Cambridge, (2001).
26. B. A. Kupershmidt, *KP or mKP*, Vol. 78 of *Mathematical Surveys and Monographs*. American Mathematical Society, Providence, RI, 2000. Noncommutative mathematics of Lagrangian, Hamiltonian, and integrable systems.
27. C. Pommerenke, Über die Faberschen Polynome schlichter Funktionen. *Math. Z.* **85**:197–208 (1964).
28. C. Pommerenke, Über die Verteilung der Fekete-Punkte. *Math. Ann.* **168**:111–127 (1967).
29. C. Pommerenke, Über die Verteilung der Fekete-Punkte. II. *Math. Ann.* **179**:212–218 (1969).
30. C. Pommerenke, *Boundary behaviour of conformal maps*, volume 299 of *Grundlehren der Mathematischen Wissenschaften [Fundamental Principles of Mathematical Sciences]*. Springer-Verlag, Berlin, 1992.
31. R. T. Rockafellar, *Convex Analysis*. Princeton Landmarks in Mathematics. Princeton University Press, Princeton, NJ, 1997. Reprint of the 1970 original, Princeton Paperbacks.
32. I. Singer, *Abstract convex analysis*. Canadian mathematical society series of monographs and advanced texts. John Wiley & Sons Inc., New York, 1997. With a foreword by A. M. Rubinov, A Wiley-Interscience Publication.
33. T. J. Stieltjes, Sur quelques théorèmes d'algèbre. *C. R. Acad Sci. Paris Sér. I Math.* **100**:620–622 (1885).
34. G. Szegö, *Orthogonal polynomials*. American mathematical society colloquium publications, Vol. 23. Revised ed. American Mathematical Society, Providence, R.I., 1959.
35. J. Thompson, *Philos. Mag* **7:**237 (1904).
36. V. Totik, *Weighted approximation with varying weight*, volume 1569 of *Lecture Notes in Mathematics*. Springer-Verlag, Berlin, 1994.
37. L. N. Trefethen, Numerical computation of the Schwarz-Christoffel transformation. *SIAM J. Sci. Stat. Comp.* **1:**82–102 (1980).
38. G. Valent and W. Van Assche, The impact of Stieltjes' work on continued fractions and orthogonal polynomials: additional material. *J. Comput. Appl. Math.* **65**(1-3):419–447 (1995).
39. E. T. Whittaker and G. N. Watson, *A Course of Modern Analysis*. Cambridge Mathematical Library. Cambridge University Press, Cambridge, 1996. An introduction to the

general theory of infinite processes and of analytic functions; with an account of the principal transcendental functions, Reprint of the fourth edition.
40. P. B. Wiegmann and A. Zabrodin, Conformal maps and integrable hierarchies. *Comm. Math. Phys.* **213**(3):523–538 (2000).